

## Signatures of collective and matter effects on supernova neutrinos at large detectors

Sandhya Choubey,<sup>1</sup> Basudeb Dasgupta,<sup>2</sup> Amol Dighe,<sup>3</sup> and Alessandro Mirizzi<sup>4</sup><sup>1</sup>*Harish-Chandra Research Institute, Chhatnag Road, Jhansi, Allahabad 211019, India*<sup>2</sup>*CCAPP, The Ohio State University, 191 W. Woodruff Avenue, Columbus 43210 Ohio, U.S.A*<sup>3</sup>*Tata Institute of Fundamental Research, Homi Bhabha Road, Mumbai 400005, India*<sup>4</sup>*II. Institut für Theoretische Physik, Universität Hamburg,  
Luruper Chaussee 149, 22761 Hamburg, Germany*

(Dated: August 1, 2010)

We calculate the expected galactic supernova neutrino signal at large next-generation underground detectors. At different epochs after the explosion, the primary fluxes can be quite different. For these primary neutrino fluxes, spectral splits induced by collective neutrino flavor transformations can arise for either mass hierarchy in both neutrino and antineutrino channels. We classify flux models according to the nature and number of these splits, and calculate the observable  $\nu_e$  and  $\bar{\nu}_e$  spectra at Earth, taking into account subsequent matter effects. We find that some of the spectral splits could occur sufficiently close to the peak energies to produce significant distortions in the observable SN neutrino signal. The most striking signature of this effect would be presence of peculiar energy dependent modulations associated with Earth matter crossing, present only in portions of the SN neutrino energy spectra demarcated by spectral splits. These signatures at proposed large water Cherenkov, scintillation, and liquid Argon detectors could give hints about the primary SN neutrino fluxes, as well as on the neutrino mass hierarchy and the mixing angle  $\theta_{13}$ .

PACS numbers: 14.60.Pq, 97.60.Bw

## I. INTRODUCTION

Observable effects of supernova (SN) neutrinos<sup>1</sup> in underground detectors are a subject of intense investigation in astroparticle physics. In particular, a lot of attention has been devoted to possible signatures of the Mikheyev-Smirnov-Wolfenstein (MSW) matter effect [1] on neutrino flavor evolution [2–4]. Shock-wave effects in the stellar envelope [6–18] and the neutrino Earth matter crossing [19–25] have been predicted to have dramatic effects on SN neutrino oscillations and to produce signatures that could allow us to extract valuable information on the unknown neutrino mass and mixing parameters, like the neutrino mass hierarchy and the mixing angle  $\theta_{13}$ .

In the recent years, it has been understood that the paradigm of neutrino flavor transformations in supernovae, based on the only MSW effect with the ordinary matter [19], was incomplete. Novel phenomena have been found to be important in the region close to the neutrinosphere, where the neutrino density is so high that effects of neutrino-neutrino interactions dominate the flavor evolution. These effects have been understood and characterized in an increasingly realistic way in a long series of papers [26–73].

The neutrino-neutrino interactions provide a large potential for the neutrinos due to the neutrinos themselves, which causes large and rapid conversions between different flavors. The transitions occur collectively, i.e. in a coherent fashion, over the entire energy range. Unlike

ordinary neutrino oscillations, these collective oscillations depend strongly on the original SN neutrino fluxes. In a supernova  $\nu_e$  and  $\bar{\nu}_e$  are distinguished from other flavors due to their additional charged-current interactions. The  $\nu_{\mu,\tau}$  and their antiparticles, on the other hand, are produced at practically identical rates. Following the standard terminology, we define the two relevant non-electron flavor states as  $\nu_{x,y} = \cos\theta_{23}\nu_\mu \mp \sin\theta_{23}\nu_\tau$ , where  $\theta_{23} \simeq \pi/4$  is the atmospheric mixing angle. Since the initial  $\nu_x$  and  $\nu_y$  fluxes are identical, the primary neutrino fluxes are best expressed in terms of  $\nu_e$ ,  $\bar{\nu}_e$  and  $\nu_x$ . The collective pair conversions  $\nu_e\bar{\nu}_e \leftrightarrow \nu_{x,y}\bar{\nu}_{x,y}$  take place even for extremely small mixing angles within the first  $\mathcal{O}(500)$  km [34], much before the MSW flavor conversions start. In a typical supernova, enough asymmetry between neutrino and antineutrino number fluxes is expected, thus complicated angle-dependent decoherence effects due to the anisotropic neutrino emission in the SN environment are likely to be suppressed [37]. There may be however a slow-down of collective flavor conversions due to multi-angle effects in deep supernova regions [72].

During the accretion phase ( $t \lesssim 0.5$  ms after the core-bounce) in typical supernova simulations [74–78] one finds an almost perfectly equipartitioned luminosity between the neutrino flavors:  $L_{\nu_e} \approx L_{\bar{\nu}_e} \approx L_{\nu_x}$ . This has been the benchmark scenario in most studies of collective flavor oscillations, which predicts: For normal mass hierarchy (NH)  $\nu$  and  $\bar{\nu}$  remain unaffected by collective oscillations. For Inverted hierarchy (IH), the end of collective oscillations is marked by an almost complete exchange of the  $\bar{\nu}_e$  and  $\bar{\nu}_y$  flavor spectra for  $\bar{\nu}$ 's, while for  $\nu$ 's the swap occurs only above a characteristic energy fixed by lepton number conservation, giving rise to a spectral split in the  $\nu$  energy distributions [38, 40, 57].

<sup>1</sup> Neutrinos will refer to both neutrinos ( $\nu$ ) and antineutrinos ( $\bar{\nu}$ ) in this article.

It is not obvious that the neutrino fluxes maintain their approximate equipartition even at late times. Indeed, the deleptonization of the core is probably faster than the cooling of the proto-neutron star, so that the asymmetry between the fluxes can become smaller and the spectra at late times depend on details of the neutrino transport (the density and the temperature profiles, as well as the treatment of the interaction rates). Due to this complexity, results from SN simulations are not unambiguous. Late-time cooling calculations performed by the Garching group [76] show a cross-over of the different neutrino luminosities  $L_{\nu_x} \gtrsim L_{\nu_e} \approx L_{\bar{\nu}_e}$ , i.e. at late times the  $\nu_x$  flux becomes relatively larger [77]. Similar results, but less pronounced, have also been obtained recently by the Basel group [78] and in the most recent long-time simulations of the Garching group [79].

This latter case ( $L_{\nu_x} \gtrsim L_{\nu_e} \approx L_{\bar{\nu}_e}$ ) was recently studied [62, 70, 71], and one found the occurrence of unexpected multiple spectral swaps and consequent spectral splits for both  $\nu$ 's and  $\bar{\nu}$ 's in either mass hierarchy. The lesson from this result is that the benchmark scenario (one spectral split in  $\nu_e$  spectrum and complete swap in the  $\bar{\nu}_e$  for inverted hierarchy) is in fact a special case, while the phenomenology of the spectral features can be more complex. To this end, a detailed study has been performed in [63], where the impact of the variations of the neutrino luminosities has been explored, finding abrupt changes in the number and the position of the splits by slightly changing the ratio between the luminosities of the different neutrino species around some critical value.

Given the sensitivity of the self-induced spectral splits on the original SN neutrino emission features, their detection in a galactic SN neutrino burst could provide a tool to reconstruct the original neutrino fluxes. Since spectral splits could potentially affect both neutrinos and antineutrinos, it seems worthwhile to investigate complementary detection techniques with sensitivity to  $\nu_e$  and  $\bar{\nu}_e$  respectively. Around the world, there is an active discussion about the feasibility of three different classes of large underground detectors for low-energy neutrino physics and astrophysics, *viz.* water Cherenkov detectors with fiducial masses ranging from  $\mathcal{O}(0.4 \text{ Mt})$  [80–82] to 5 Mt [83], liquid scintillation detectors with masses of  $\mathcal{O}(50 \text{ kt})$  [84] and liquid Argon Time Projection Chambers (LAr TPC) with fiducial masses of  $\mathcal{O}(100 \text{ kt})$  [85–88]. In particular, these three detection techniques are the backbones of the European project LAGUNA (Large Apparati for Grand Unification and Neutrino Astrophysics) [89] and the LBNE (Long Baseline Neutrino Experiment) in DUSEL (Deep Underground Science and Technology Laboratory) [90]. The physics potential of such devices for supernova neutrino detection would be extremely high. In particular, water Cherenkov and scintillation neutrino experiments are mostly sensitive to supernova  $\bar{\nu}$  through the inverse beta decay process  $\bar{\nu}_e + p \rightarrow e^+ + n$ . On the other hand, LAr TPC would have a high sensitivity to SN  $\nu$ , through the charged current

interactions of  $\nu_e$  with the Ar nuclei in the detector. The complementarity between these different detection techniques would allow to compare the different features, like the spectral splits, occurring in SN neutrino spectra.

Motivated by this intriguing perspective, our aim in this paper is to calculate the observable SN signal at these detectors. The main feature of our work is an improved treatment of the oscillation physics, particularly collective effects, in different phases of the SN explosion. We also investigate the detectability of possible features in the observable galactic supernova signal at future large underground detectors and examine the physics potential.

The plan of the article is as follows. In Sec. II, we describe the parameter space of expected primary neutrino fluxes, the equations for the neutrino flavor evolution, and neutrino mixing. In Sec. III, we give a short overview of the collective effects on neutrino spectra and the multiple spectral splits. We also perform a scan on the SN flux parameter space to identify different classes of fluxes that lead to qualitatively different final spectra. Sec. IV discusses the subsequent flavor conversions due to MSW effects and possible Earth matter effects, and presents the net survival probabilities for  $\nu_e$  and  $\bar{\nu}_e$  arriving at the detectors. In Sec. V, we describe the features of our reference detectors (fiducial mass, cross sections and energy resolution). In Sec. VI we present our results on the detectability of the spectral signatures in the  $\nu_e$  and  $\bar{\nu}_e$  signal. In particular, we discuss the distinctive features due to interplay of Earth matter effects and spectral splits. We also briefly comment on neutrino oscillation effects on the early neutronization burst and in relation to the SN shock-wave propagation. Finally, in Sec. VII we comment about our results, discuss future perspectives, and conclude.

## II. FLUXES, POTENTIALS AND MIXING PARAMETERS

In this section, we describe the primary fluxes, the effective potentials they encounter during their propagation, and the neutrino mixing parameters that we use in our numerical simulations.

### A. Primary neutrino fluxes

The primary neutrino fluxes of all neutrino and antineutrino species can be written as

$$F_\nu^0(E) = \Phi_\nu^0 \varphi(E), \quad (1)$$

where  $\nu = \nu_e, \bar{\nu}_e, \nu_x$ ,  $\varphi(E)$  is the normalized primary neutrino spectrum, i.e.  $\int dE \varphi(E) = 1$ , and  $\Phi_\nu^0$  is the total number flux. For  $\varphi(E)$  we use the spectral

parameterization given in Ref. [76]:

$$\varphi(E) = \frac{(\alpha_\nu + 1)^{(\alpha_\nu + 1)}}{\Gamma(\alpha_\nu + 1)} \left( \frac{E}{\langle E_\nu \rangle} \right)^{\alpha_\nu} \frac{e^{-(\alpha_\nu + 1)E/\langle E_\nu \rangle}}{\langle E_\nu \rangle}, \quad (2)$$

where  $\langle E_\nu \rangle$  is the average  $\nu$  energy,  $\alpha_\nu$  is a spectral parameter, and  $\Gamma$  is the Euler gamma function. The values of the parameters are model dependent [74, 75]. There is significant variation across different SN simulations, but we find that the  $\langle E_{\nu_e} \rangle$  and  $\langle E_{\bar{\nu}_e} \rangle$  are usually close to

$$\langle E_{\nu_e} \rangle = 12 \text{ MeV} \text{ and } \langle E_{\bar{\nu}_e} \rangle = 15 \text{ MeV}, \quad (3)$$

whereas  $\langle E_{\nu_x} \rangle$  tends to vary in the range

$$16 \text{ MeV} \leq \langle E_{\nu_x} \rangle \leq 25 \text{ MeV}. \quad (4)$$

We fix the spectral pinching parameter at  $\alpha_\nu = 3$  for all species.

The total number fluxes  $\Phi_\nu^0$  are related to the luminosities of the neutrino species through

$$\Phi_\nu^0 = \frac{L_\nu}{\langle E_\nu \rangle}. \quad (5)$$

For definiteness, we assume a typical supernova which emits  $E_B \approx 3 \times 10^{53}$  erg in a duration of  $t = 10$  s. The time integrated luminosities of all species combined is equal to the total emitted energy:

$$\int dt (L_{\nu_e} + L_{\bar{\nu}_e} + 4L_{\nu_x}) = E_B, \quad (6)$$

such that the average number fluxes are about  $10^{55} \text{ s}^{-1} \text{ MeV}^{-1}$ , and about  $10^{58}$  neutrinos are emitted in the entire SN explosion.

The ratio between the different luminosities varies significantly across models, but we find that (See Fig.3 of [63] and Table 7.3 of [91] for example)

$$\begin{aligned} L_{\nu_e}/L_{\bar{\nu}_e} &\approx 1, \\ 0.5 &\lesssim L_{\nu_x}/L_{\nu_e} \lesssim 2.0. \end{aligned} \quad (7)$$

The relative number fluxes change over the duration of the neutrino burst. In particular, the fluxes in the accretion phase are not necessarily similar to those in the cooling phase. These primary fluxes are subject to flavor conversions, of which the collective oscillations that we will discuss in the next section depend quite sensitively on the fluxes themselves.

## B. Neutrino equations of motion

Mixed neutrinos are described by matrices of density  $\rho_{\mathbf{p}}$  and  $\bar{\rho}_{\mathbf{p}}$  for each (anti)neutrino mode. The diagonal entries are the usual occupation numbers whereas the off-diagonal terms encode phase information. The equations of motion (EoMs) are [92]

$$i\partial_t \rho_{\mathbf{p}} = [\mathbf{H}_{\mathbf{p}}, \rho_{\mathbf{p}}], \quad (8)$$

where the Hamiltonian is

$$\mathbf{H}_{\mathbf{p}} = \Omega_{\mathbf{p}} + \mathbf{V}_{\text{MSW}} + \mathbf{V}_{\nu\nu}. \quad (9)$$

Here  $\Omega_{\mathbf{p}}$  is the matrix of the vacuum oscillation frequencies for neutrinos, which is

$$\Omega_{\mathbf{p}} = \text{diag}(m_1^2, m_2^2, m_3^2)/2|\mathbf{p}| \quad (10)$$

in the mass basis. For antineutrinos  $\Omega_{\mathbf{p}} \rightarrow -\Omega_{\mathbf{p}}$ . The matter effect due to the background electron density  $n_e$  is, in the weak interaction basis, i.e.  $(\nu_e, \nu_\mu, \nu_\tau)$ ,

$$\mathbf{V}_{\text{MSW}} = \sqrt{2}G_F n_e \text{diag}(1, 0, 0), \quad (11)$$

neglecting the second-order difference between the  $\nu_\mu$  and  $\nu_\tau$  refractive indices that could be important for collective neutrino oscillations only at really early post-bounce times ( $t \lesssim 300$  ms) [46, 93].

The effective potential due to the neutrino-neutrino interactions is

$$\mathbf{V}_{\nu\nu} = \sqrt{2}G_F \int \frac{d^3\mathbf{q}}{(2\pi)^3} (\rho_{\mathbf{q}} - \bar{\rho}_{\mathbf{q}})(1 - \mathbf{v}_{\mathbf{p}} \cdot \mathbf{v}_{\mathbf{q}}), \quad (12)$$

where  $\mathbf{v}_{\mathbf{p}}$  is the velocity of the neutrino mode  $\mathbf{p}$ .

In spherical symmetry the EoMs can be expressed as a closed set of differential equations along the radial direction [37, 53]. The factor  $(1 - \mathbf{v}_{\mathbf{q}} \cdot \mathbf{v}_{\mathbf{q}})$  in the Hamiltonian gives rise to ‘‘multi-angle’’ effects for neutrinos moving on different trajectories [33]. However, for realistic supernova conditions the modifications are presumably small (except for a shift in the onset of the flavor conversions [72]), allowing for a single-angle approximation [37, 60]. We implement this approximation by assuming all neutrinos to have been launched from the neutrinosphere at radius  $R$ , with an angle  $45^\circ$  relative to the radial direction [37, 46]. In this case, the formal derivation of the single-angle approximation explicitly gives the radial dependence of the neutrino-neutrino interaction strength as [53]

$$\mathbf{V}_{\nu\nu}(r) \propto \mu(r) = \mu_0 \frac{R^2}{r^2} C_r. \quad (13)$$

Here,  $\mu_0$  is the interaction strength

$$\mu_0 = \sqrt{2}G_F (F_{\nu_e}^0 - F_{\bar{\nu}_e}^0), \quad (14)$$

the  $r^{-2}$  scaling comes from the geometrical flux dilution, while the collinearity factor

$$\begin{aligned} C_r &= 4 \left[ \frac{1 - \sqrt{1 - (R/r)^2}}{(R/r)^2} \right]^2 - 1 \\ &= \frac{1}{2} \left( \frac{R}{r} \right)^2 \quad \text{for } r \rightarrow \infty \end{aligned} \quad (15)$$

arises from the  $(1 - \mathbf{v}_{\mathbf{p}} \cdot \mathbf{v}_{\mathbf{q}})$  structure of the neutrino-neutrino interaction. The decline of the neutrino-neutrino interaction strength,  $\mu(r) \sim r^{-4}$  for  $r \gg R$ ,

is evident, while the numerical coefficient for large  $r$  depends on the launching angle, here taken to be  $45^\circ$ . When fluxes at the neutrinosphere radius  $R = 10$  km are taken, we get

$$\mu_0 = 7 \times 10^5 \text{ km}^{-1} . \quad (16)$$

Of course, the physical neutrinosphere is not a well-defined concept. Therefore, the radius  $R$  simply represents the location where we fix the inner boundary conditions. However, essentially nothing happens close to the neutrinosphere because the in-medium mixing angle is extremely small. Therefore, as far as the vacuum and matter oscillation terms are concerned, it is almost irrelevant where we fix the inner boundary condition.

### C. Neutrino mixing parameters

We work in the rotated basis [47]

$$(\nu_e, \nu_x, \nu_y) \equiv \mathbf{R}^T(\theta_{23})(\nu_e, \nu_\mu, \nu_\tau) .$$

This is equivalent to taking  $\theta_{23} = 0$  in the neutrino mixing matrix, which makes no difference to  $\nu_e$  and  $\bar{\nu}_e$  evolution as long as the primary fluxes of  $\nu_\mu$  and  $\nu_\tau$  are identical, as we have assumed. The values of the other mixing angles are  $\sin^2 \theta_{12} \simeq 0.30$  and  $\sin^2 \theta_{13} \lesssim 0.04$  [94] in vacuum. The neutrino mass-squared differences in vacuum are taken to be  $\Delta m_{\text{atm}}^2 = 2 \times 10^{-3} \text{ eV}^2$  and  $\Delta m_{\text{sol}}^2 = 7.6 \times 10^{-5} \text{ eV}^2$ , close to their current best-fit values [94]. We study both the cases of normal neutrino mass hierarchy (NH:  $\Delta m_{\text{atm}}^2 = m_3^2 - m_{1,2}^2 > 0$ ) and inverted mass hierarchy (IH:  $\Delta m_{\text{atm}}^2 = m_3^2 - m_{1,2}^2 < 0$ ). We ignore possible subleading CP violating effects [55] by setting  $\delta_{\text{CP}} = 0$ .

Matter effects in the region of collective oscillations (up to a few 100 km) suppress the mixing angles and slightly modify the neutrino mass-square differences. We take the matter-suppressed mixing angles to be  $\tilde{\theta}_{13} = \tilde{\theta}_{12} = 10^{-3}$  and the effective mass-square differences  $\Delta \tilde{m}_{\text{atm}}^2 = \Delta m_{\text{atm}}^2 \cos \theta_{13} \simeq \Delta m_{\text{atm}}^2$  and  $\Delta \tilde{m}_{\text{sol}}^2 = \Delta m_{\text{sol}}^2 \cos \theta_{12} \simeq 0.4 \Delta m_{\text{sol}}^2$  [48, 54]. Apart from these shifts, matter effects typically do not disturb the development of the collective neutrino oscillations, except at very early times ( $t \lesssim 300$  ms) when the effective electron density  $n_e$  would become larger than the neutrino density  $n_\nu$ , suppressing the collective flavor conversions [54]. For simplicity, in the following we will always focus on later times where collective oscillations are not inhibited by a strong matter term. MSW conversions occur after collective effects have ceased [47, 60, 61]. Therefore, their effects factorize, and will be described in Sec. IV.

## III. COLLECTIVE FLAVOR CONVERSIONS

Although the subject of collective oscillations has been discussed in great detail in number of papers, most have

focused on the benchmark scenario used in [42]. It was pointed out in [62, 70, 71] that the final outcome of collective effects can be quite complicated, depending on the primary fluxes. In this section we will perform a detailed study investigating the effect of the primary fluxes on flavor oscillations during the different post-bounce phases.

### A. Spectral swaps and splits

Near the neutrinosphere, due to the large neutrino density, the neutrino-neutrino interaction energy is very large. This ensures that neutrinos exhibit collective oscillations, i.e. neutrinos of all energies oscillate coherently with the same average frequency. As the neutrinos stream outward and the neutrino density becomes smaller, self-induced oscillations begin to take place [34]. These oscillations, being instability driven, have a large amplitude even for a very small mixing angle. In the presence of a slowly decreasing background neutrino density, the collective effects on the neutrinos become negligible beyond a point, and their imprint on the spectra is left in the form of the spectral splits. The energy and the number of the splits is crucially dependent on the neutrino mass hierarchy (normal or inverted), and on the relative sizes of the primary number fluxes of different flavors.

The resultant dynamics of the spectral splits has been elaborated in [62, 71]: spectral swaps can develop around *unstable crossing points*. Here crossing points are those energies  $E_c$  where spectra of different flavors cross each other, i.e.

$$F_{\nu_e}^0(E_c) = F_{\nu_x}^0(E_c) \quad \text{or} \quad F_{\bar{\nu}_e}^0(E_c) = F_{\bar{\nu}_x}^0(E_c) . \quad (17)$$

A given crossing point is unstable for  $e \leftrightarrow y$  (“atmospheric sector”) swap, triggered by  $(\Delta m_{\text{atm}}^2, \theta_{13})$ , if at the energy  $E_c$ ,

$$\begin{aligned} d(F_{\nu_e}^0 - F_{\nu_x}^0)/dE &< 0 \quad \text{for IH} , \\ d(F_{\nu_e}^0 - F_{\nu_x}^0)/dE &> 0 \quad \text{for NH} , \end{aligned} \quad (18)$$

and analogously for antineutrinos. Thus, in IH we get a  $\nu_e \leftrightarrow \nu_y$  or  $\bar{\nu}_e \leftrightarrow \bar{\nu}_y$  swap around every crossing with a negative slope, while in NH we get such a swap around every crossing with a positive slope. Each swap is demarcated by two spectral splits. Two subtle points may be noted: (i) If two unstable crossings are very close to each other, the swaps may be influenced by each other and even merge, and (ii) If an unstable crossing is too closely flanked by stable crossings, the width of the swap around it is suppressed exponentially, which also leads to adiabaticity violation leading to smearing out of that swap [62].

In addition, a crossing point is unstable for the  $e \leftrightarrow x$  (“solar sector”) swap, triggered by  $(\Delta m_{\text{sol}}^2, \theta_{12})$ , if [71]

$$d(F_{\nu_e}^0 - F_{\nu_x}^0)/dE > 0 , \quad (19)$$

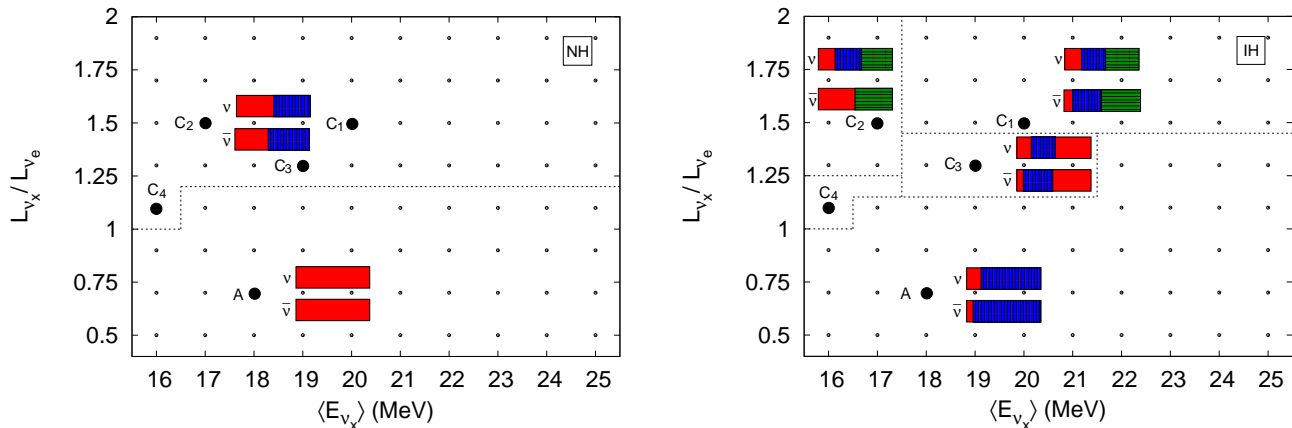


FIG. 1: Regions of the flux parameter space that produce qualitatively different spectra after collective flavor transformations. Left panel for NH, Right for IH. The bands represent the positions of spectral swaps in energy, and their nature: vertical stripes correspond to  $\nu_e \leftrightarrow \nu_y$  swap, horizontal stripes correspond to  $\nu_e \leftrightarrow \nu_x$  swap, unstriped regions have no swap. The widths of the striped / unstriped regions approximately indicate the energy range where they are present, the complete band corresponding to the energy range 1-50 MeV.

and analogously for antineutrinos. We thus obtain a  $\nu_e \leftrightarrow \nu_x$  or  $\bar{\nu}_e \leftrightarrow \bar{\nu}_x$  swap around every crossing with a positive slope. These swaps tend to be more non-adiabatic than those in the atmospheric sector, since the natural frequency of the solar sector,  $\Delta m_{\text{sol}}^2/(2E)$ , is smaller than that of the atmospheric sector. As a result, the rate of change of the collective interaction strength may become too fast for there to be enough time for the solar sector instability to grow.

The combination of the atmospheric and solar sector swaps may give rise to three-flavor effects, pointed out recently in [70, 71]. For NH, mass splittings are positive in both the atmospheric and solar sectors, and both the mixing angles are small due to matter suppression. Both the sectors then tend to produce instabilities at the same energies, but the atmospheric sector wins due to its higher natural frequency (and hence larger adiabaticity). As a result, only  $\nu_e \leftrightarrow \nu_y$  and  $\bar{\nu}_e \leftrightarrow \bar{\nu}_y$  swaps develop, and no three-flavor effects are observed. On the other hand, in IH the atmospheric and solar instabilities are in different parts of the spectrum. The solar sector instability then operates in the high-energy region without hindrance and causes an additional swap that may even merge with the atmospheric sector swap, partially erasing one of the spectral splits. However, the split usually is not completely erased because of the non-adiabaticity of the swap in the solar sector.

## B. Flux dependence of spectral splits

The number and positions of the spectral splits depends on the primary neutrino spectra [63]. However a clear mapping between primary fluxes and split patterns is still lacking. The flux parameters with the widest

variation among models are the average energy of the  $\nu_x$  flux  $\langle E_{\nu_x} \rangle$ , and the  $\nu_x$  luminosity  $L_{\nu_x}$ . We scan the SN neutrino parameter space in the variables  $L_{\nu_x}/L_{\nu_e}$  and  $\langle E_{\nu_x} \rangle$  in the ranges defined by Eqs. (4) and (7), and numerically evolve the system of neutrinos to determine the regions of the flux parameter space where different spectral swaps are effective. We then classify the primary spectra depending on the number and nature of these swaps.

The results of this classification may be represented by a “phase diagram” shown in Fig. 1. Note that the idea of a phase diagram, in which the oscillation patterns change abruptly across regions, has been implemented earlier in [63, 67] where a two-flavor analysis of collective effects is carried out. Our survey involves a three-flavor treatment of collective effects, and is carried out over a different slice of the parameter space, i.e. we allow the  $\nu_x$  energies to vary while fixing  $L_{\bar{\nu}_e} = L_{\nu_e}$ . The surveys in Ref. [63, 67] chose to fix the  $\nu_x$  energy and vary the relative fluxes / luminosities of the flavors. Our choice is motivated by the observation that most simulations tend to predict  $L_{\nu_e} \approx L_{\bar{\nu}_e}$ , whereas  $\langle E_{\nu_x} \rangle$  turns out to be much less robustly predicted. We therefore believe that this survey provides useful information that is complementary to the one in [63, 67].

From the phase diagram, it is observed that for NH, there are two phases with qualitatively different split patterns. Phase A, which approximately corresponds to  $L_{\nu_e} \gtrsim L_{\nu_x}$ , shows no spectral swaps in  $\nu$  or  $\bar{\nu}$ . On the other hand, in the other phase C with  $L_{\nu_e} \lesssim L_{\nu_x}$ , one obtains a  $\nu_e \leftrightarrow \nu_y$  swap and a  $\bar{\nu}_e \leftrightarrow \bar{\nu}_y$  swap, both at energies  $\gtrsim 25$  MeV. The situation is more complicated for IH. Here the phase A, which is approximately the same as the phase A in NH, corresponds to a  $\nu_e \leftrightarrow \nu_y$  swap at energies  $\gtrsim 8$  MeV, and a  $\bar{\nu}_e \leftrightarrow \bar{\nu}_y$  swap at

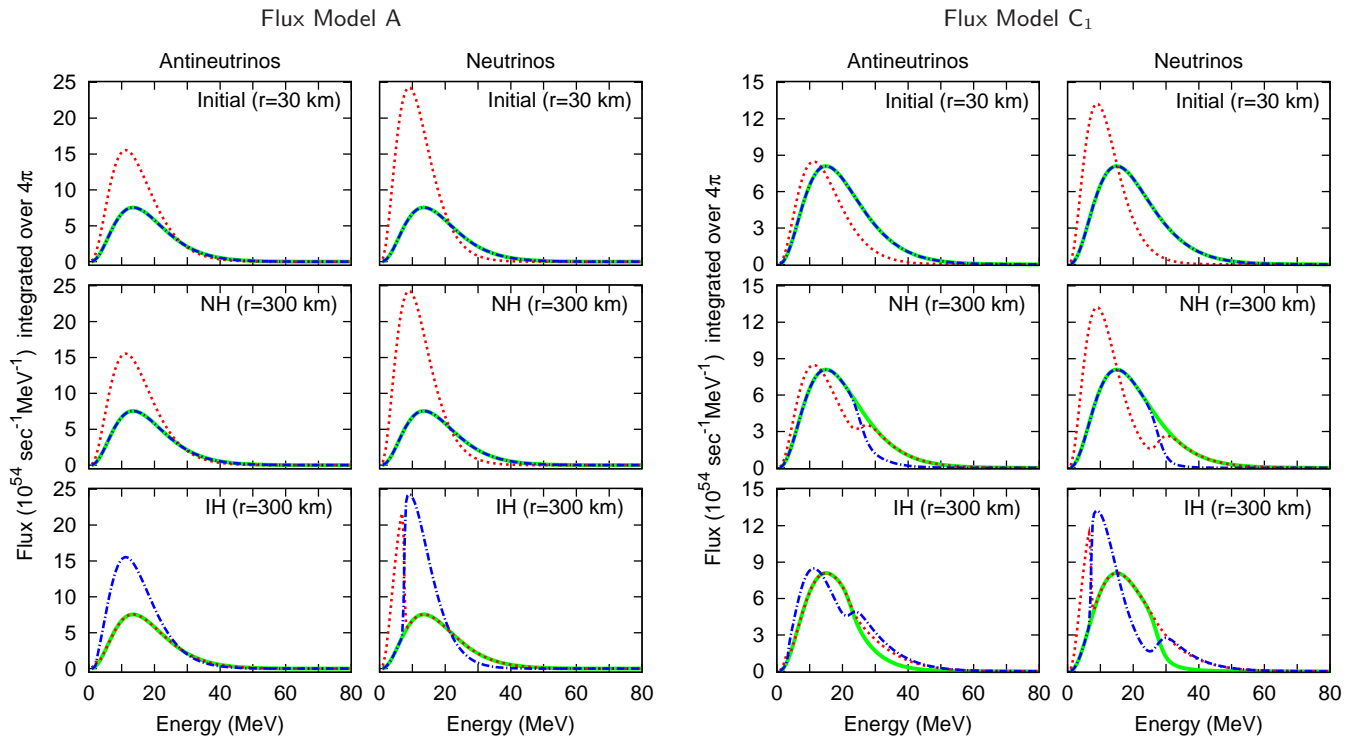


FIG. 2: Fluxes (integrated over  $4\pi$  solid angle) for the benchmark models: A (left panel),  $C_1$  (right panel). In each panel, fluxes are shown for antineutrinos (left) and neutrinos (right) at initial time at neutrinosphere (top), post-collective oscillations in IH (middle) and NH (bottom). The  $e$  flavor is shown in red/dotted,  $x$  in green/solid, and  $y$  in blue/dot-dashed. The fluxes for models  $C_2$ ,  $C_3$ ,  $C_4$  are not shown, as they are similar to  $C_1$ , with certain features degraded (see text).

energies  $\gtrsim 4$  MeV. The phase C however has different features depending on its sub-phases  $C_1$ ,  $C_2$ ,  $C_3$  and  $C_4$ .

- $C_1$  corresponds to a large  $L_{\nu_x}$  and large  $\langle E_{\nu_x} \rangle$ , and hence here the spectral swaps are more pronounced. Both  $\nu_e \leftrightarrow \nu_y$  as well as  $\bar{\nu}_e \leftrightarrow \bar{\nu}_y$  swaps appear at intermediate energies  $10 \text{ MeV} \lesssim E \lesssim 25 \text{ MeV}$ . For  $E \gtrsim 25 \text{ MeV}$ , there are  $\nu_e \leftrightarrow \nu_x$  and  $\bar{\nu}_e \leftrightarrow \bar{\nu}_x$  swaps.
- In  $C_2$ , the energy  $\langle E_{\nu_x} \rangle$  is lower as compared to  $C_1$ . Then  $\bar{\nu}_e$  and  $\bar{\nu}_y$  spectra are very similar at intermediate energies. As a result, the  $\bar{\nu}_e \leftrightarrow \bar{\nu}_y$  swap at intermediate energies has low adiabaticity, and is not effective.
- In  $C_3$ , the luminosity  $L_{\nu_x}$  is lower as compared to  $C_1$ . Then the  $\nu_e$  and  $\nu_x$  spectra, as well as the  $\bar{\nu}_e$  and  $\bar{\nu}_x$  spectra, are very similar at high energies. As a result, the  $\nu_e \leftrightarrow \nu_x$  and  $\bar{\nu}_e \leftrightarrow \bar{\nu}_x$  swaps at high energies have low adiabaticity, and are not effective.
- $C_4$  corresponds to almost equal  $\bar{\nu}_e$  and  $\bar{\nu}_x$  number fluxes everywhere except at intermediate energies near the peaks. As a result, the  $\nu_e \leftrightarrow \nu_x$  and  $\bar{\nu}_e \leftrightarrow \bar{\nu}_x$  swaps at high energies are non-adiabatic and hence ineffective. The  $\nu_e \leftrightarrow \nu_y$  and  $\bar{\nu}_e \leftrightarrow \bar{\nu}_y$  swaps at intermediate energies are partially adiabatic. This case can be thought to be the combination of  $C_2$  and  $C_3$ , with only the common features surviving.

In Fig. 2, we illustrate the spectral swaps for two benchmark points

$$\begin{aligned} \text{A} : \langle E_{\nu_x} \rangle &= 18 \text{ MeV}, L_{\nu_x}/L_{\nu_e} = 0.7, \\ \text{C}_1 : \langle E_{\nu_x} \rangle &= 20 \text{ MeV}, L_{\nu_x}/L_{\nu_e} = 1.5. \end{aligned} \quad (20)$$

The benchmark point A lies close to the predictions of the Garching flux model [75] during accretion phase, while  $C_1$  lies close to the predictions during cooling phase. Here we show the primary fluxes of all  $\nu$  as well as  $\bar{\nu}$  species, and show how they change after collective effects. The  $\nu_e$  and  $\bar{\nu}_e$  spectra after collective oscillations exhibit the spectral features described before. We point out that for the  $C_1$  flux, in IH the oscillated  $\nu_e$  spectrum shows a single split, the one at low-energy, corresponding to the swap with  $\nu_y$ , while the high-energy split is canceled by the further  $\nu_e \leftrightarrow \nu_x$  swap. However, this high-energy split is still visible in the  $\nu_x$  and  $\nu_y$  spectra. We will see in the following that this high-energy split would reappear in the final  $\nu_e$  spectrum at Earth, since that is a superposition of the different  $\nu$  spectra after collective oscillations. The same observations apply for the  $\bar{\nu}_e$  spectrum. Moving from the case  $C_1$  to  $C_4$  in the phase C one may observe a gradual degradation in the observability of the different spectral splits in final spectra (not shown).

## IV. FLUXES AFTER MSW CONVERSIONS

### A. Survival probabilities

After collective oscillation die out, the primary neutrino fluxes  $F_\nu^0$  experience spectral swaps and then further undergo the traditional MSW conversions in SN [19, 95] while passing through the resonance regions  $H$  and  $L$ , corresponding to flavor transitions in the two-neutrino sectors associated with  $(\Delta m_{\text{atm}}^2, \theta_{13})$  and  $(\Delta m_{\text{sol}}^2, \theta_{12})$ , respectively. After exiting the resonance regions, the neutrino mass eigenstates travel independently until they reach Earth, wherein they are detected as flavor eigenstates. The fluxes of  $\nu_e$  and  $\bar{\nu}_e$  arriving at Earth can be written as [19]

$$\begin{aligned} F_{\nu_e} &= pF_{\nu_e}^0 + (1-p)F_{\nu_x}^0, \\ F_{\bar{\nu}_e} &= \bar{p}F_{\bar{\nu}_e}^0 + (1-\bar{p})F_{\bar{\nu}_x}^0, \end{aligned} \quad (21)$$

where  $p$  and  $\bar{p}$  are the  $\nu_e$  and  $\bar{\nu}_e$  survival probabilities, respectively. The survival probabilities are determined by the adiabaticity of the MSW  $H$ -resonance and in general are sensitive to the neutrino energy and to the SN matter density profile (see, e.g., [8]). This dependence vanishes for a large time-window in the limiting cases of adiabatic transitions ( $\sin^2 \theta_{13} \gtrsim 10^{-3}$ ) and strongly non-adiabatic transitions ( $\sin^2 \theta_{13} \lesssim 10^{-5}$ ) (see, e.g., [24]). In the following, we shall consider for simplicity only these two limiting cases.

In these two regions of the  $\theta_{13}$  parameter space, the expressions for  $p$  and  $\bar{p}$  can be written down in a simple form, as shown in Tables I and II. The survival probabilities have been given separately for the low-energy ( $E < E_{\text{low}}$ ), intermediate energy ( $E_{\text{low}} < E < E_{\text{high}}$ ) and high-energy ( $E > E_{\text{high}}$ ) regions. Here  $E_{\text{low}}$  and  $E_{\text{high}}$ , respectively, are the energies where the low-energy and high-energy spectral splits are likely to be present. For  $\nu_e$ , one has  $E_{\text{low}} \approx 10$  MeV and  $E_{\text{high}} \approx 25$  MeV. For  $\bar{\nu}_e$ , one gets  $E_{\text{low}} \approx 5$  MeV and  $E_{\text{high}} \approx 25$  MeV. The survival probabilities also depend on the primary fluxes, and are given for the phases A ( $L_{\nu_e} \gtrsim L_{\nu_x}$ ) and C ( $L_{\nu_e} \lesssim L_{\nu_x}$ ), covering the complete parameter space. Some special subcases of C are given in the caption. These are related to the cases C<sub>2</sub>, C<sub>3</sub>, C<sub>4</sub> shown in Fig. 1, for which we have seen that some of the splits can be suppressed by the presence of too close  $\bar{\nu}_e$  and  $\bar{\nu}_x$  spectra or by the low  $\nu_x$  luminosity.

Note that the survival probability is never 1. The vacuum mixing due to the angle  $\theta_{12}$  always mixes the  $\nu_e$  or  $\bar{\nu}_e$  spectra with the other flavors. Effects of the spectral swaps are invariably reduced by a factor of  $\sin^2 \theta_{12} \approx 0.3$  or  $\cos^2 \theta_{12} \approx 0.7$ .

### B. Earth matter effect

The neutrino survival probabilities at the Earth given in Tables I and II are calculated assuming that neutrinos

escaping the star travel through vacuum before reaching the detector. If the supernova is shadowed by the Earth for a detector, the neutrinos will travel a certain distance through the Earth, and will undergo Earth matter oscillations during this propagation. Since the neutrinos arrive at the Earth as mass eigenstates, the net effect of these oscillations can be written in terms of the conversion probabilities  $P_{ie} = P(\nu_i \rightarrow \nu_e)$ . Neglecting the effect due to small  $\theta_{13}$ , one can obtain the net survival probabilities by the substitution [19]

$$(\cos^2 \theta_{12}, \sin^2 \theta_{12}) \rightarrow (1 - P_{2e}, P_{2e}) \quad (22)$$

for neutrinos in Table I, and

$$(\cos^2 \theta_{12}, \sin^2 \theta_{12}) \rightarrow (1 - \bar{P}_{2e}, \bar{P}_{2e}) \quad (23)$$

for antineutrinos in Table II. Here

$$P_{2e} \equiv P(\nu_2 \rightarrow \nu_e), \quad \text{and} \quad \bar{P}_{2e} \equiv P(\bar{\nu}_2 \rightarrow \bar{\nu}_e) \quad (24)$$

while propagating through the Earth. Analytical expressions for  $P_{2e}$  and  $\bar{P}_{2e}$  can be calculated for the approximate two-density model of the Earth [23]. When neutrinos traverse a distance  $L$  through only the mantle of the Earth, these quantities have a very simple form [19, 20]:

$$P_{2e} = \sin^2 \theta_{12} + \sin 2\theta_{12}^m \times \quad (25)$$

$$\sin(2\theta_{12}^m - 2\theta_{12}) \sin^2 \left( \frac{\Delta m_{\text{sol}}^2 \sin 2\theta_{12}}{4E \sin 2\theta_{12}^m} L \right),$$

$$\bar{P}_{2e} = \sin^2 \theta_{12} + \sin 2\bar{\theta}_{12}^m \times \quad (26)$$

$$\sin(2\bar{\theta}_{12}^m - 2\theta_{12}) \sin^2 \left( \frac{\Delta m_{\text{sol}}^2 \sin 2\theta_{12}}{4E \sin 2\bar{\theta}_{12}^m} L \right),$$

where  $\theta_{12}^m$  and  $\bar{\theta}_{12}^m$  are the effective values of  $\theta_{12}$  in Earth matter for neutrinos and antineutrinos, respectively [95].

The Earth crossing thus induces an oscillatory signature in the neutrino energy spectrum. However note that these oscillations are absent if the corresponding survival probabilities vanish: they occur only when  $p \neq 0$  or  $\bar{p} \neq 0$  in Tables I and II. Depending on the swap pattern, the Earth effect can then appear in different energy regions in the spectra. As we shall see in Sec. VI, the mere observation of Earth matter effects is sometimes enough to distinguish between different flux and mixing scenarios.

## V. NEUTRINO DETECTION

In this section we describe the main aspects and ingredients of our calculations of supernova neutrino event rates. The oscillated SN neutrino fluxes at Earth,  $F_\nu$ , must be convolved with the differential cross section  $\sigma_e$  for electron or positron production, as well as with the energy resolution function  $R_e$  of the detector, and

TABLE I: Survival probability  $p$  for  $\nu_e$  at low, intermediate and high energies, for fluxes in phase A and C. Within phase C, the exceptions to the rule are denoted by the brackets (..) for  $C_3$  and  $C_4$ .

		Phase A ( $L_{\nu_e} \gtrsim L_{\nu_x}$ )			Phase C ( $L_{\nu_e} \gtrsim L_{\nu_x}$ )		
		$E < E_{\text{low}}$	$E_{\text{low}} < E < E_{\text{high}}$	$E > E_{\text{high}}$	$E < E_{\text{low}}$	$E_{\text{low}} < E < E_{\text{high}}$	$E > E_{\text{high}}$
NH	$\sin^2 \theta_{13} \gtrsim 10^{-3}$	0	0	0	0	0	$\sin^2 \theta_{12}$
	$\sin^2 \theta_{13} \lesssim 10^{-5}$	$\sin^2 \theta_{12}$	$\sin^2 \theta_{12}$	$\sin^2 \theta_{12}$	$\sin^2 \theta_{12}$	$\sin^2 \theta_{12}$	0
IH	$\sin^2 \theta_{13} \gtrsim 10^{-3}$	$\sin^2 \theta_{12}$	0	0	$\sin^2 \theta_{12}$	0	$\cos^2 \theta_{12} (\sin^2 \theta_{12})$
	$\sin^2 \theta_{13} \lesssim 10^{-5}$	$\sin^2 \theta_{12}$	0	0	$\sin^2 \theta_{12}$	0	$\cos^2 \theta_{12} (\sin^2 \theta_{12})$

TABLE II: Survival probability  $\bar{p}$  for  $\bar{\nu}_e$  at low, intermediate and high energies, for fluxes in phases A and C. Within phase C, the exceptions to the rule are denoted by: brackets (..) for  $C_3$  and  $C_4$ , square brackets [..] for  $C_2$  and  $C_4$ .

		Phase A ( $L_{\nu_e} \gtrsim L_{\nu_x}$ )			Phase C ( $L_{\nu_e} \gtrsim L_{\nu_x}$ )		
		$E < E_{\text{low}}$	$E_{\text{low}} < E < E_{\text{high}}$	$E > E_{\text{high}}$	$E < E_{\text{low}}$	$E_{\text{low}} < E < E_{\text{high}}$	$E > E_{\text{high}}$
NH	$\sin^2 \theta_{13} \gtrsim 10^{-3}$	$\cos^2 \theta_{12}$	$\cos^2 \theta_{12}$	$\cos^2 \theta_{12}$	$\cos^2 \theta_{12}$	$\cos^2 \theta_{12}$	0
	$\sin^2 \theta_{13} \lesssim 10^{-5}$	$\cos^2 \theta_{12}$	$\cos^2 \theta_{12}$	$\cos^2 \theta_{12}$	$\cos^2 \theta_{12}$	$\cos^2 \theta_{12}$	0
IH	$\sin^2 \theta_{13} \gtrsim 10^{-3}$	0	$\cos^2 \theta_{12}$	$\cos^2 \theta_{12}$	0	$\cos^2 \theta_{12} [0]$	$\sin^2 \theta_{12} (0)$
	$\sin^2 \theta_{13} \lesssim 10^{-5}$	$\cos^2 \theta_{12}$	0	0	$\cos^2 \theta_{12}$	0 [ $\cos^2 \theta_{12}$ ]	$\sin^2 \theta_{12} (\cos^2 \theta_{12})$

the efficiency  $\varepsilon$ , in order to finally get observable event rates [11]:

$$N_e = F_\nu \otimes \sigma_e \otimes R_e \otimes \varepsilon . \quad (27)$$

To calculate the total number of events, we will assume the supernova distance  $d = 10$  kpc and integrate the event rates over  $t = 10$  s, assuming the fluxes to be constant over the entire duration. The fluxes are thus to be thought of as the time-averaged fluxes over 10 s. Alternately a more detailed modeling of the time-dependent flux is required, in which case a time-binned analysis may be performed.

We will now describe the main characteristics of three types of detectors: water Cherenkov detectors, scintillation detectors, and liquid Argon Time Projection Chambers, that we have used to calculate the signals.

### A. Water Cherenkov detectors

In large water-Cherenkov detectors, the golden channel for supernova neutrino detection is the inverse beta decay of electron antineutrinos <sup>2</sup>

$$\bar{\nu}_e + p \rightarrow n + e^+ . \quad (28)$$

For this process, we take the differential cross section from [96]. The total cross section grows approximatively

as  $E^2$ . We fold the differential cross sections for  $e^+$  production with a Gaussian energy resolution function of width  $\Delta$ . The value of  $\Delta$  is predominantly determined by the photocathode coverage of the detector. For our calculations we assume [9, 97]

$$\Delta_{\text{WC}}/\text{MeV} = 0.47\sqrt{E_e/\text{MeV}} , \quad (29)$$

where  $E_e$  is the true positron energy. A galactic SN is expected to produce  $\mathcal{O}(10^5)$  events in a Mt-class water Cherenkov detector with a fiducial volume of about 400 kt [89].

### B. Scintillation detectors

In liquid scintillators, the main channel for SN neutrino detection is the inverse beta decay of  $\bar{\nu}_e$ 's, the same as that in water Cherenkov. However, here the positrons are detected through photons produced in the scintillation material. Since a larger number of photons can be produced in a scintillation detector, these have typically a much better energy resolution than the water Cherenkov detectors. Indeed, the energy resolution of a scintillation detector may be better by more than a factor of 6. The energy resolution of the scintillator detectors is determined by the number of photo-electrons produced per MeV, which for this type of detectors is expected to be given by as good as [98, 99]

$$\Delta_{\text{SC}}/\text{MeV} = 0.075\sqrt{E_e/\text{MeV}} . \quad (30)$$

Since the Earth matter oscillations described in the previous section may get smeared out by the finite energy resolution of the detector, it is clear that the energy

<sup>2</sup> We will neglect the subleading neutrino interaction channels in the detectors, assuming that they can be separated at least on a statistical basis.



resolution plays a crucial role in the efficiency of detecting Earth effects. For a fiducial mass of 50 kt, one expects  $\mathcal{O}(10^4)$  events for a galactic SN [89].

### C. Liquid Argon Time Projection Chambers

LAr TPC detectors would be particularly sensitive to SN electron neutrinos through their charged current interactions with Argon nuclei

$$\nu_e + {}^{40}\text{Ar} \rightarrow {}^{40}\text{K}^* + e^- , \quad (31)$$

which proceed via the creation of an excited state of  ${}^{40}\text{K}$  and its subsequent gamma decay. The Q-value for this inverse beta decay process is 1.505 MeV. The cross-section for this charged current reaction is taken from [100]. Energy resolution in such detectors is expected to be very good. The energy resolution for leptons in liquid argon time projection chambers has been calculated by the ICARUS collaboration who report [101]

$$\Delta_{\text{LAr}}/\text{MeV} = 0.11\sqrt{E_e/\text{MeV}} + 0.02 E_e/\text{MeV} . \quad (32)$$

The fiducial volume for supernova neutrino detection is taken to be 100 kt [102]. With these standard inputs, one expects  $\mathcal{O}(10^4)$  events from the interactions considered above [89], while the event rates produced by the other interaction channels are smaller by at least an order of magnitude. Due to the strong sensitivity to  $\nu_e$ , the liquid Argon technique would be complementary to the water Cherenkov and scintillation detectors, which are mostly sensitive to  $\bar{\nu}_e$ 's.

## VI. OBSERVABLES SENSITIVE TO NEUTRINO FLAVOR CONVERSIONS

In this Section we discuss about possible signatures of SN neutrinos flavor conversions observable in the neutrino energy spectra in the three different types of detectors, presented before. First we calculate the neutrino energy spectra at different detectors and we discuss about the observability of the spectral splits and of the Earth matter effect. Then, we also comment about two other possible observables sensitive to the neutrino mixing, namely the  $\nu_e$  prompt neutronization burst and the shock-wave effect on the SN neutrino signal.

In order to get a realistic idea of what features of the neutrino spectra can be observable at a neutrino detector, we show the events observable at different detectors for two of our benchmark cases, A and C<sub>1</sub>, in Figures 3 and 4, respectively. For the  $\nu_e$  spectra, we show the events at a LAr TPC, while for the  $\bar{\nu}_e$  spectra, we use the scintillation detector. The events spectra at the water Cherenkov can be obtained by smearing the  $\bar{\nu}_e$  spectra at the scintillation detector. We do not show them separately in this figure. The event-rates will scale

as  $E_B/d^2$  and the volume of the detector, and one can read off the statistical errors, that go as  $\sqrt{N}$ , accordingly.

We now analyze features in the detected neutrino spectra that can tell us about the flux and mixing scenarios, and examine the feasibility of detection of these features under different conditions.

### A. Spectral splits

Spectral splits are produced at the boundaries of swaps, as shown in Fig. 2. At a spectral split, the survival probability  $p$  or  $\bar{p}$  jumps suddenly, so that a sharp jump in the spectrum is in principle observable if the primary spectra of electron and non-electron flavors at the split energy are different. The magnitude of the jump is reduced by the nonzero value of  $\theta_{12}$ , and its sharpness is somewhat smeared out by the energy resolution as well as possible non-adiabatic nature of the swap.

Figures 3 and 4 bring out the following features of the spectral split:

- In the phase A, collective oscillations occur in IH, producing a spectral split in the  $\nu$ 's and a complete swap of  $\bar{\nu}$ 's. However, the split energy is relatively low (around 10 MeV). At this energy, the difference in  $F_{\nu_e}$  and  $F_{\nu_x}$  is small, and the charged current  $\nu_e$ -Ar cross section, being  $\propto E^2$ , is also small. As a result, this “classic” spectral split in phase A is practically unobservable, as can be seen in Fig. 3. We realize that the peculiar interplay between collective and MSW effects can lead to quite different neutrino spectra for the two mass hierarchies and for large and small values of  $\theta_{13}$ . However, lacking of a calibration of the original SN neutrino fluxes, in this case it would be hard to make any strong statement about neutrino mixing just from the observation of the neutrino energy spectra.
- Observable spectra produced by  $\nu$  with primary fluxes as in C<sub>1</sub> are represented in Fig. 4. In the phase C, splits are possible in both,  $\nu_e$  and  $\bar{\nu}_e$  spectra at higher energies, around  $E_{\text{split}} = 25$  MeV. This is near the peak of the primary spectra, so the difference between the electron and non-electron flavor spectra is more pronounced. This makes possible the detection of signatures related to spectral splits. In particular for  $\bar{\nu}_e$ , in NH and in IH with  $\sin^2 \theta_{13} \gtrsim 10^{-3}$ , the observable positron spectrum in a liquid scintillation detector (or in a water Cherenkov detector) is mostly due to  $F_{\bar{\nu}_e}^0$  for  $E < E_{\text{split}}$  and  $F_{\nu_x}^0$  at higher energies (see Table II). This would produce a bimodal positron spectrum, with two peaks corresponding to the two peaks of the initial antineutrino distributions. Instead, at  $\sin^2 \theta_{13} \lesssim 10^{-5}$  in IH, the positron spectrum above  $E \simeq 10$  MeV will be mostly produced by  $F_{\bar{\nu}_x}^0$

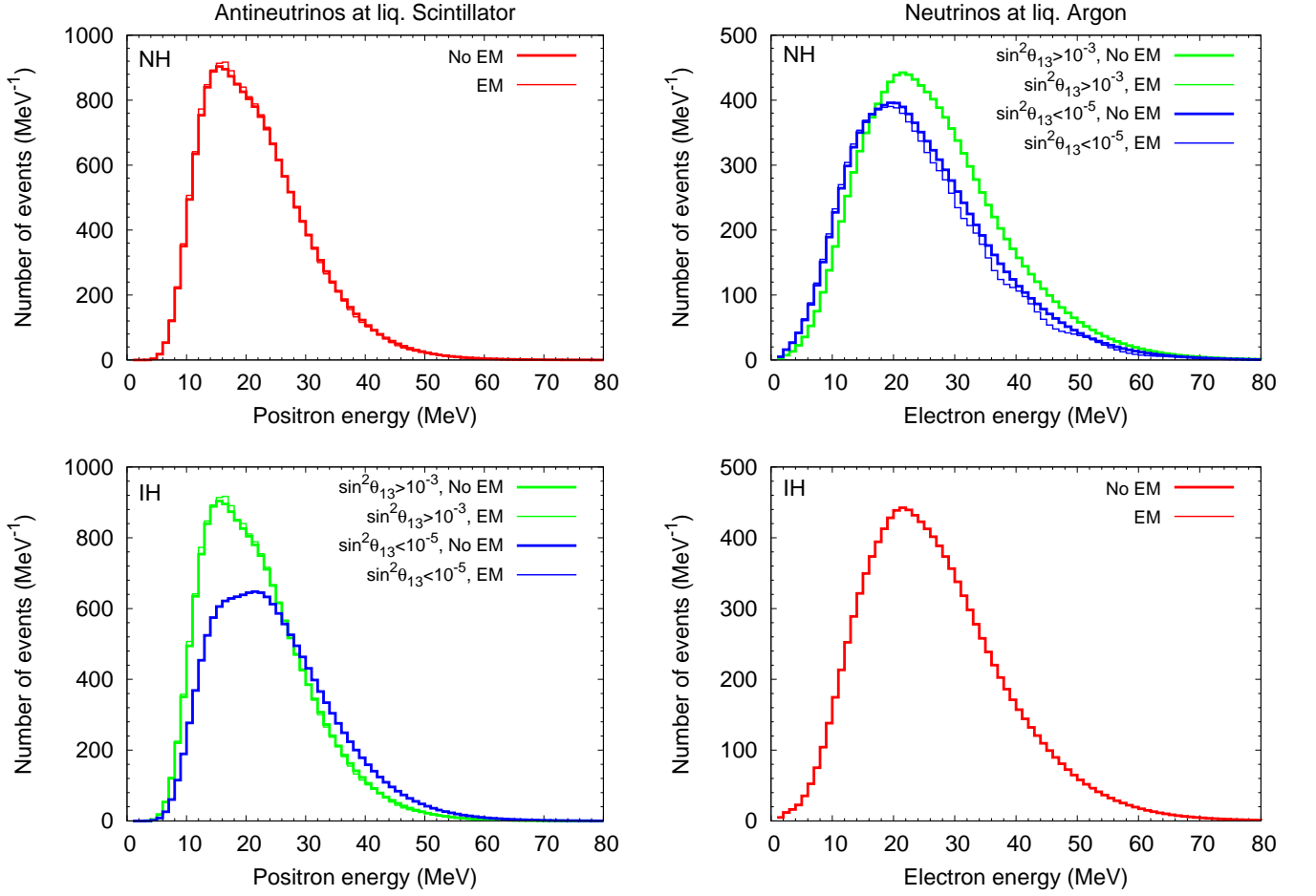


FIG. 3: For benchmark flux model A,  $\bar{\nu}_e$  and  $\nu_e$  energy spectra at 50 kt scintillator and 100 kt LAr TPC detectors, in both the hierarchies NH (upper panels) and IH (lower panels), with and without oscillations due to Earth matter effects. The spectra with Earth matter effects (EM) have been calculated for  $L = 8000$  km through the Earth, and have been denoted by thinner lines. The spectra at a water Cherenkov detector can be obtained by smearing the energy of  $\bar{\nu}_e$  at the scintillator detector, and multiply the number of events  $\sim 10$  times.

(see Table II), therefore no special spectral feature seems to be visible.

Concerning the electron spectrum produced by SN  $\nu_e$  in a LAr TPC, in NH and  $\sin^2 \theta_{13} \lesssim 10^{-5}$ , we observe a bimodal distribution produced by a superposition of  $F_{\nu_e}^0$  and  $F_{\nu_x}^0$  for  $E \lesssim E_{\text{split}}$  and by mostly  $F_{\nu_x}^0$  at high energies (see Table I), producing a broad “shoulder”. Instead, in NH and  $\sin^2 \theta_{13} \gtrsim 10^{-3}$  the electron spectrum will be mostly produced by the  $F_{\nu_x}^0$ . This is qualitatively similar to what happens also in IH.

The presence of bimodal distributions and broad “shoulder” features in the spectra produced by  $\nu_e$  and  $\bar{\nu}_e$  for the  $C_1$  primary flux, then hold the promise of being observable at the detectors, in spite of the energy smearing.

- In  $C_2$  the average energies of  $\bar{\nu}_e$  and  $\bar{\nu}_x$  are similar, as a result only one peak would be observed; the

shoulder may not be discernible. Similarly in  $C_3$  and  $C_4$ , since the number fluxes of electron and non-electron flavors are close to each other, direct observation of the spectral split is hard.

In summary, the spectral splits are directly identifiable only in the phase C, when the average energy and luminosity of non-electron fluxes are sufficiently large.

## B. Earth matter effect

As discussed in Sec. IV B, the passage of neutrinos through the Earth before reaching the detector can give rise to Earth matter effect oscillations in the spectra. For definiteness, in the following we will assume the neutrino path length in the Earth to be  $L = 8000$  km.

From Eqs. (25) and (26), these oscillations have frequencies that are functions only of the solar neutrino mixing parameters, and hence are well known. It is then

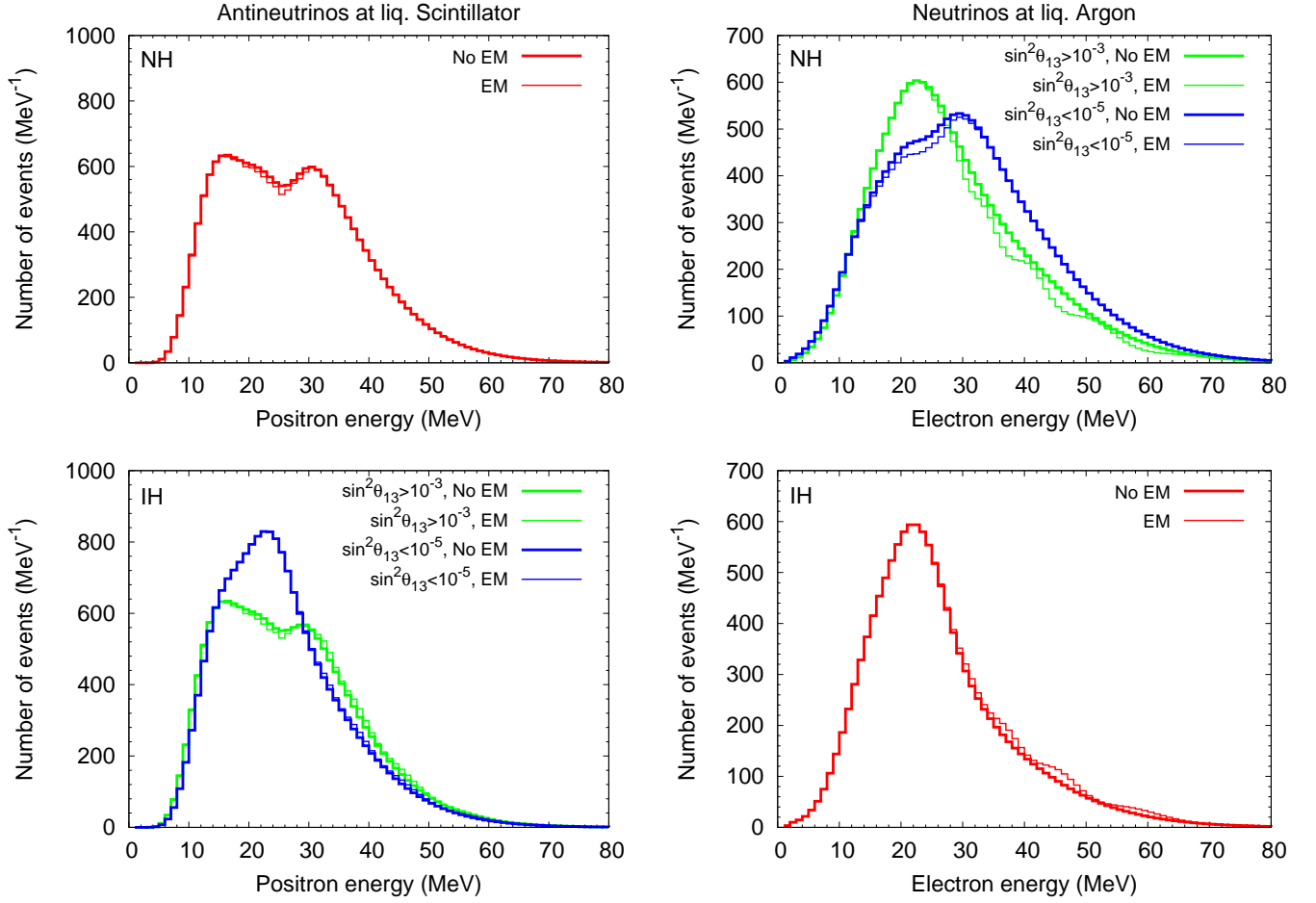


FIG. 4: The same as Fig. 3, but for the benchmark flux model  $C_1$ .

simply a question of identifying the oscillations in the final spectra, if they exist. As can be seen in Figs. 3 and 4, scintillation detectors and LAr TPCs can allow us to detect these spectral modulations. The following statements can be made from Table I and II and from Figures 3 and 4:

- For the phase A, oscillations are expected in the  $\nu_e$  spectrum for NH with  $\sin^2 \theta_{13} \lesssim 10^{-5}$ . These oscillations should be clearly detectable in LAr TPC. For NH with  $\sin^2 \theta_{13} \gtrsim 10^{-3}$ , as well as for IH, there are no expected Earth effects in the  $\nu_e$  spectrum.
- For the phase A, oscillations are expected in the  $\bar{\nu}_e$  spectrum for IH with  $\sin^2 \theta_{13} \gtrsim 10^{-3}$  and in NH. However in this case, the small flux differences between original antineutrino species leads to the presence of Earth induced oscillations at high energies being barely visible, as can be seen from Fig. 3. The mixing scenarios IH with  $\sin^2 \theta_{13} \lesssim 10^{-5}$  will not produce any Earth effects.
- For  $C_1$ , Earth effects in  $\nu_e$  spectrum are expected in all mixing scenarios (See Table I). In particular,

for NH with  $\sin^2 \theta_{13} \lesssim 10^{-5}$ , the Earth effects are only at intermediate energies (10–25 MeV), while for the other mixing scenarios, they are prominent at high energies ( $E > 25$  MeV). The sign of these effects is negative in NH and positive in IH. In particular, as one can see from Fig. 4, that the Earth matter modulations are clearly visible in the electron spectrum at high energies. This is due to the fact that in this case the spectral differences between  $F_{\nu_e}^0$  and  $F_{\nu_x}^0$  are relatively large at high energies.

- For the case  $C_1$ , Earth effects in  $\bar{\nu}_e$  are prominent at high energies if the hierarchy is IH. For NH, the effects are expected at intermediate energies. However, due to the smaller spectral differences between  $F_{\bar{\nu}_e}^0$  and  $F_{\bar{\nu}_x}^0$  these features are difficult to be observed, as can be seen from the Figure.
- For  $C_2$ ,  $C_3$  and  $C_4$  – not shown in Figs. 3 and 4 – the Earth matter effects are in general less pronounced than in  $C_1$ . This is a result of some of the swaps being absent or only partially adiabatic.

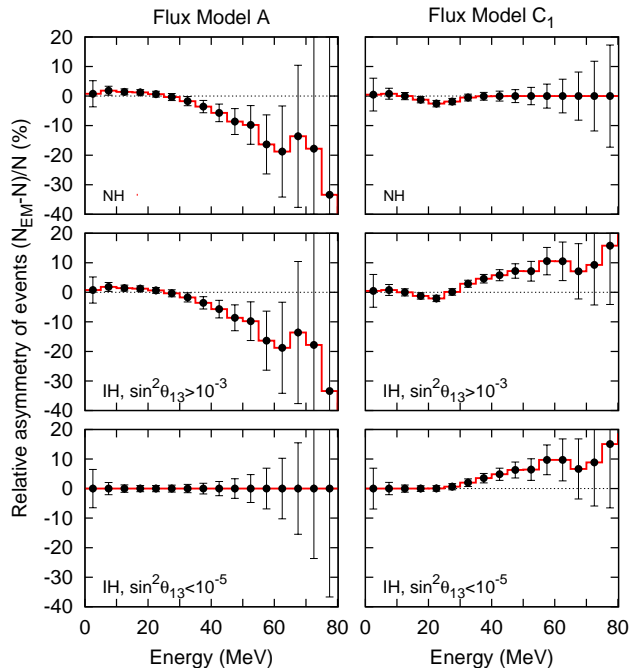


FIG. 5: The left panel shows the relative asymmetry of  $\bar{\nu}_e$  events with and without Earth matter effects at two 0.4 Mt water Cherenkov detectors, for the benchmark flux model A. For Earth effects, the distance travelled through the Earth is taken to be 8000 km. In the right panel we show the same ratio for the benchmark flux model  $C_1$ .

The above observations are consistent with the prediction that the Earth effects would appear only at those energies where the survival probabilities  $p$  or  $\bar{p}$  in Tables I and II are nonzero.

The Earth induced modulations can be identified at a single scintillation or LAr TPC detector by the Fourier Transform technique [22, 23]. Clear observation of Earth effect oscillations in  $\nu_e$  would then correspond to the possibilities (i) primary fluxes A, and NH with  $\sin^2 \theta_{13} \lesssim 10^{-5}$  (ii) primary fluxes C. Observation of Earth effect oscillations in  $\bar{\nu}_e$  flux at the shadowed detector is more likely for primary fluxes C, but may be possible for A as well. The combination of the Earth effect signals in  $\nu_e$  and  $\bar{\nu}_e$  may then enable us to shortlist the possible combinations of the flux and mixing scenarios. The Earth effects are visible in the intermediate or high energy range depending on the flux and mixing scenario. If one is able to divide a spectrum into energy regions where Earth effects are present and where they are not, further distinction between flux and mixing scenarios is possible. However practically this task looks very hard. Also, note that non-detection of the Earth effects may be either due to their non-existence or simply due to their being too small to be detected. Therefore, in general the non-observation of these oscillations would not give us any concrete information.

On the other hand, at a water Cherenkov detector whose energy resolution may be insufficient for discerning

the oscillations, one may rely on comparison between signals at two detectors. It is quite possible that we will have more than one large water Cherenkov detectors within a couple of decades. Moreover, IceCube can be used as an accurate luminosity calibrator, and comparing the time dependence of luminosity in IceCube with that in another large water Cherenkov can help us identify Earth effects even without resolving the oscillations [103]. Figure 5 shows some scenarios where the Earth effects may be observable without identification of oscillations, through the comparison between two detectors or the comparison between two different signals at the same detector. A combination of two 0.4 Mt-class water Cherenkov detectors, one shadowed by the Earth and the other unshadowed [25], has the capability to distinguish the mass hierarchies in the phase A for  $\sin^2 \theta_{13} < 10^{-5}$ , through an overall suppression of the event rate at the shadowed detector for NH [49]. In phase C, this combination can identify the hierarchies through the enhancement of high-energy events at the shadowed detector. Note that one of the two detectors could in fact be IceCube, as we do not really need the energy dependence.

### C. Suppression of $\nu_e$ in the neutronization burst

The primary signal during the early neutronization burst ( $t \lesssim 20$  ms) is pure  $\nu_e$ . Since the model predictions for the energy and luminosity of the burst are fairly robust [104], the observation of the burst signal gives direct information about the survival probability of  $\nu_e$ . This probability is  $\mathcal{O}(\theta_{13}^2)$  in NH with  $\sin^2 \theta_{13} \gtrsim 10^{-3}$ , and  $\sin^2 \theta_{12}$  in all the other scenarios [19]. Thus, the strong suppression of  $\nu_e$  burst would be a smoking gun signal for the former scenario. Note that since no  $\bar{\nu}$  are involved, self-induced oscillations are not developed and hence the collective effects do not give rise to any flavor transformations during the neutronization burst.

However, in low-mass O-Ne-Mg supernovae ( $M \simeq 8 - 10 M_\odot$ ), the MSW resonances may lie deep inside the collective regions during the neutronization burst, when the neutrino luminosity is even higher. In such a situation, neutrinos of all energies undergo the MSW resonances together, with the same adiabaticity [105]. As long as this adiabaticity is nontrivial, one gets the “MSW-prepared spectral splits”, two for normal hierarchy and one for inverted hierarchy [43, 44, 48, 73]. The positions of the splits can be predicted from the primary spectra [44]. The splits imply  $\nu_e$  suppression that is stepwise in energy. Such a signature may even be used to identify the O-Ne-Mg supernova, in addition to identifying the hierarchy. A LAr TPC with good timing and energy resolution would play a crucial role in this. However, we leave the study of this particular case for a future work.

#### D. Shock-wave effects

Observables like the number of events, average energy, or the width of the spectrum may display dips or peaks for short time intervals, while the shock wave is passing through the  $H$ -resonance. The positions of the dips or peaks in the number of events at different neutrino energies would also allow one to trace the shock propagation while the shock is in the mantle, around densities of  $\rho \sim 10^3$  g/cc [9, 11]. The interplay between collective oscillations and shock-wave signatures has been recently studied in [61]. This information, by itself or in combination with the corresponding gravitational wave signal, will yield valuable information about the SN explosion, in addition to confirming  $\sin^2 \theta_{13} \gtrsim 10^{-3}$  and identifying NH (if the effects are seen in the  $\nu_e$  spectrum) or IH (if the effects are seen in the  $\bar{\nu}_e$  spectrum) as the actual hierarchy. A caveat in this context is the role of matter turbulences in the post-shock regions and their impact on neutrino flavor conversions. Presumably, these would at least partially erase the signatures of the shock-waves in the neutrino signal [13, 15–18].

### VII. SUMMARY AND CONCLUSIONS

In this paper we have performed the first detailed study of the impact of collective and matter-induced flavor oscillations in the interpretation of the observable SN neutrino signal at a large water Cherenkov detector, a scintillation detector, and a Liquid Argon Time Projection Chamber. We have analyzed the neutrino flavor evolution, including collective effects that give rise to spectral swaps and the MSW effects that further mix the neutrino flavors. In particular, we have taken into account the possible qualitative change in the fluxes and oscillation physics during the SN neutrino emission. We have calculated the neutrino flux at Earth, including possible Earth matter effects introduced if the neutrinos pass through the Earth before reaching the detector. We have also calculated the  $\nu_e$  and  $\bar{\nu}_e$  spectra through the dominant channels at the above detectors, taking care of the detector efficiencies and energy resolutions.

The collective effects, which are dominant for  $r \lesssim 500$  km, leave their imprints in the form of spectral swaps. The boundaries of spectral swaps are spectral splits, where the  $\nu_e$  or  $\bar{\nu}_e$  spectra can have sharp jumps at critical energy values. Since the collective effects are essentially nonlinear, the number and position of these splits depends on the primary neutrino spectra. To explore this, we have fixed the average energies for  $\nu_e$  and  $\bar{\nu}_e$  fluxes, assuming that their luminosities are almost equal (a result borne out by many SN neutrino simulations), and we have scanned the parameter space in the average energy and luminosity of the non-electron neutrinos. It turns out that, depending on the number and nature of spectral swaps, the parameter space may be divided into two main “phases”: the phase A ( $L_{\nu_x} \lesssim L_{\nu_e}$ )

that is typical of the fluxes during accretion, and the phase C ( $L_{\nu_x} \gtrsim L_{\nu_e}$ ) that is typical of the fluxes during cooling. Phase A shows no spectral swap in NH while in IH shows a spectral swap at intermediate (10 MeV  $\lesssim E \lesssim 25$  MeV) and high ( $E \gtrsim 25$  MeV) energies for both  $\nu$  and  $\bar{\nu}$ . Phase C, on the other hand, shows spectral swap in both  $\nu$  as well as  $\bar{\nu}$  at high energies even in NH. In IH it in general results in two spectral swaps, a  $e \leftrightarrow y$  swap at intermediate energies and a  $e \leftrightarrow x$  swap at high energies.

We have also taken into account the MSW and Earth matter effects that determine the further neutrino flavor conversions after the collective effects are over. Armed with these results, we have looked for distinctive signatures of neutrino mixing pattern in the  $\nu_e$  and  $\bar{\nu}_e$  spectra at the detectors, and we have examined the feasibility of their observation. In particular, we have considered (i) the sharp change in the spectrum that is the signature of a spectral split (ii) the Earth matter effects, (iii) the flavor conversion effects on the prompt  $\nu_e$  neutronization burst, and (iv) the shock-wave effects in the neutrino as well as antineutrino spectra.

The spectral split itself will be visible only if the corresponding survival probability  $p$  or  $\bar{p}$  changes suddenly at an energy  $\gtrsim 10$  MeV. While the splits in phase A only occur at low energies, the splits in phase C can occur at intermediate energies and can be observable. These splits will be a clear signature of the collective effects taking place deep inside the star, since no other known phenomenon can give rise to such a sharp change in the neutrino spectrum. Typically, the presence of spectral splits would produce bimodal observable energy spectral with two peaks corresponding to the ones of the initial  $\nu_e$  and  $\nu_x$  spectra. Our results for the other observables are summarized in Tables III and IV.

From the tables, it can be observed that

- Whether the Earth effects are visible at intermediate energies, high energies, or not at all, depends on the neutrino mass hierarchy and the range of  $\theta_{13}$ . A clear identification of the Earth effects is therefore crucial in extracting neutrino mixing information from the observed spectra. (Note that since the threshold of the detectors will be  $\sim 5$  MeV, we have ignored any effects at low energies.) If the Earth effects are present in the intermediate energy range and absent in the high energy range (or vice versa), it will be a signature of a spectral split. Thus, an indirect observation of a spectral split is also possible through Earth matter effects.
- The vanishing of  $\nu_e$  burst and the observation of shock wave effects is independent of the collective effects. These observables thus directly probe the neutrino mixing pattern: mass hierarchy and  $\theta_{13}$  range.

Concerning our study, we would to remind that while we have modeled the SN fluxes, and treated their oscillations in more detail than have been done in previous

TABLE III: Observable effects in the  $\nu_e$  spectra, for fluxes of type A and C. Earth effects at low energies ( $E \lesssim 10$  MeV) are almost impossible to detect and have not been considered.

		Phase A ( $L_{\nu_e} \gtrsim L_{\nu_x}$ )			Phase C ( $L_{\nu_e} \gtrsim L_{\nu_x}$ )		
		$\nu_e$ burst	Earth effects	Shock effects	$\nu_e$ burst	Earth effects	Shock effects
NH	$\sin^2 \theta_{13} \gtrsim 10^{-3}$	Vanishes	Absent	Possible	Vanishes	Only high $E$	Possible
	$\sin^2 \theta_{13} \lesssim 10^{-5}$	Present	All $E$	Absent	Present	Only intermediate $E$	Absent
IH	$\sin^2 \theta_{13} \gtrsim 10^{-3}$	Present	Absent	Absent	Present	Only high $E$	Absent
	$\sin^2 \theta_{13} \lesssim 10^{-5}$	Present	Absent	Absent	Present	Only high $E$	Absent

TABLE IV: Observable effects in the  $\bar{\nu}_e$  spectra, for fluxes of type A and C. The exceptions in region C are: with fluxes in regions C<sub>3</sub> and C<sub>4</sub> and IH. Earth effects are absent for  $\sin^2 \theta_{13} \gtrsim 10^{-3}$ , while they are present at intermediate as well as high energies for  $\sin^2 \theta_{13} \lesssim 10^{-5}$ . Earth effects at low energies ( $E \lesssim 10$  MeV) are almost impossible to detect and have not been considered.

		Phase A ( $L_{\nu_e} \gtrsim L_{\nu_x}$ )		Phase C ( $L_{\nu_e} \gtrsim L_{\nu_x}$ )	
		Earth effects	Shock effects	Earth effects	Shock effects
NH	$\sin^2 \theta_{13} \gtrsim 10^{-3}$	All $E$	Absent	Only intermediate $E$	Absent
	$\sin^2 \theta_{13} \lesssim 10^{-5}$	All $E$	Absent	Only intermediate $E$	Absent
IH	$\sin^2 \theta_{13} \gtrsim 10^{-3}$	Intermediate and high $E$	Possible	Intermediate and high $E$	Possible
	$\sin^2 \theta_{13} \lesssim 10^{-5}$	Absent	Absent	Only high $E$	Absent

literature, the results shown here are for a simplified treatment of the SN neutrino problem which ignores possible trajectory-dependent effects, inhomogeneities, etc. All these effects would potentially introduce additional layers of complications in the simulation of the supernova neutrino signal and their impact will need careful dedicated studies. In this sense, we believe that the predictions of possible signatures of supernova neutrino oscillations in large underground detectors need further investigations. This task is particularly timely now when different classes of large underground detectors are currently under study for low-energy neutrino astrophysics and long-baseline experiments. In particular, from the perspective of supernova neutrinos it would be extremely useful to have as many different detection techniques as possible.

We would like to emphasize that the information obtained from the SN  $\nu_e$  spectrum is as crucial as that obtained from the  $\bar{\nu}_e$  spectrum, and in some cases even more useful. For example, the difference between the fluxes  $F_{\nu_e}^0$  and  $F_{\nu_x}^0$  is always much more than the difference between the fluxes  $F_{\bar{\nu}_e}^0$  and  $F_{\bar{\nu}_x}^0$ . Therefore, the features of flavor transformations like the spectral splits and Earth effects are likely to be more prominent in the  $\nu_e$  spectrum, if present. Moreover, the shock-wave effects can be visible only in either  $\nu_e$  or  $\bar{\nu}_e$  channel, depending on the mass hierarchy. The information from the  $\nu_e$  spectrum observed at a LAr TPC would therefore be not just complementary to the one obtained from a water Cherenkov or scintillation detector, but it will also probe features of the SN neutrino signal that are not accessible to a  $\bar{\nu}_e$  detector.

We wish to stress that the physics potential of large neutrino detectors proposed for low-energy neutrino astrophysics is immense, and can be exploited further for studies of SN neutrinos. The accurate timing information obtained from water Cherenkov, scintillation and LAr TPC detectors should also allow us to track the SN  $\nu$  light curve quite faithfully. A detailed study of the time evolution of the neutrino signal could offer new insights. A LAr TPC would also be the most efficient detector for observing the  $\nu_e$  neutronization burst. A comparison between the onset timing of this signal with the onset time signals from  $\bar{\nu}_e$  [106–109] detectable in water (or ice) Cherenkov and scintillation detectors, and gravitational wave signals may shed more light on the SN dynamics and neutrino emission.

In conclusion, large future neutrino detectors would offer unprecedented opportunities to study supernova neutrinos and determine fundamental neutrino properties through high-statistics studies of energy and time spectra. With the complementary physics potential of future water Cherenkov, scintillation and liquid Argon detectors, they promise to advance our understanding of the physics of neutrinos, and of their flavor conversions during a stellar collapse.

#### Acknowledgments

A.D. was partly supported by the Max Planck - India Partner Group in Neutrino Physics and Astrophysics. A.M. was supported by the German Science Foundation (DFG) within the Collaborative Research Center 676 “Particles, Strings and the Early Universe”.

- 
- [1] L. Wolfenstein, “Neutrino Oscillations In Matter,” *Phys. Rev. D* **17**, 2369 (1978); S. P. Mikheev and A. Yu. Smirnov, “Resonance Enhancement Of Oscillations In Matter And Solar Neutrino Spectroscopy,” *Yad. Fiz.* **42**, 1441 (1985) [*Sov. J. Nucl. Phys.* **42**, 913 (1985)].
- [2] G. G. Raffelt, “Physics Opportunities With Supernova Neutrinos,” *Prog. Part. Nucl. Phys.* **64**, 393 (2010).
- [3] A. Dighe, “Supernova neutrino oscillations: what do we understand?,” *J. Phys. Conf. Ser.* **203**, 012015 (2010) [arXiv:0912.4167 [hep-ph]].
- [4] H. Duan and J. P. Kneller, “Neutrino flavour transformation in supernovae,” *J. Phys. G* **36**, 113201 (2009) [arXiv:0904.0974 [astro-ph.HE]].
- [5] R. C. Schirato and G. M. Fuller, “Connection between supernova shocks, flavor transformation, and the neutrino signal,” [arXiv:astro-ph/0205390] (unpublished).
- [6] K. Takahashi, K. Sato, H. E. Dalhed and J. R. Wilson, “Shock propagation and neutrino oscillation in supernova,” *Astropart. Phys.* **20**, 189 (2003) [arXiv:astro-ph/0212195].
- [7] C. Lunardini and A. Yu. Smirnov, “Probing the neutrino mass hierarchy and the 13-mixing with supernovae,” *JCAP* **0306**, 009 (2003) [arXiv:hep-ph/0302033].
- [8] G. L. Fogli, E. Lisi, A. Mirizzi, and D. Montanino, “Analysis of energy- and time-dependence of supernova shock effects on neutrino crossing probabilities,” *Phys. Rev. D* **68**, 033005 (2003) [arXiv:hep-ph/0304056].
- [9] R. Tomàs, M. Kachelrieß, G. Raffelt, A. Dighe, H. T. Janka and L. Scheck, “Neutrino signatures of supernova shock and reverse shock propagation,” *JCAP* **0409**, 015 (2004) [arXiv:astro-ph/0407132].
- [10] B. Dasgupta and A. Dighe, “Phase effects in neutrino conversions during a supernova shock wave,” *Phys. Rev. D* **75**, 093002 (2007) [arXiv:hep-ph/0510219].
- [11] G. L. Fogli, E. Lisi, A. Mirizzi and D. Montanino, “Probing supernova shock waves and neutrino flavor transitions in next-generation water-Cherenkov detectors,” *JCAP* **0504**, 002 (2005) [arXiv:hep-ph/0412046].
- [12] V. Barger, P. Huber and D. Marfatia, “Supernova neutrinos can tell us the neutrino mass hierarchy independently of flux models,” *Phys. Lett. B* **617**, 167 (2005) [arXiv:hep-ph/0501184].
- [13] G. L. Fogli, E. Lisi, A. Mirizzi and D. Montanino, “Damping of supernova neutrino transitions in stochastic shock-wave density profiles,” *JCAP* **0606**, 012 (2006) [arXiv:hep-ph/0603033].
- [14] S. Choubey, N. P. Harries and G. G. Ross, “Probing neutrino oscillations from supernovae shock waves via the IceCube detector,” *Phys. Rev. D* **74**, 053010 (2006) [arXiv:hep-ph/0605255].
- [15] S. Choubey, N. P. Harries and G. G. Ross, “Turbulent supernova shock waves and the sterile neutrino signature in megaton water detectors,” *Phys. Rev. D* **76**, 073013 (2007) [arXiv:hep-ph/0703092].
- [16] A. Friedland and A. Gruzinov, “Neutrino signatures of supernova turbulence,” [arXiv:astro-ph/0607244].
- [17] J. P. Kneller, G. C. McLaughlin and J. Brockman, “Oscillation Effects and Time Variation of the Supernova Neutrino Signal,” *Phys. Rev. D* **77**, 045023 (2008) [arXiv:0705.3835 [astro-ph]].
- [18] J. P. Kneller and C. Volpe, “Turbulence effects on supernova neutrinos,” [arXiv:1006.0913 [hep-ph]].
- [19] A. S. Dighe and A. Yu. Smirnov, “Identifying the neutrino mass spectrum from the neutrino burst from a supernova,” *Phys. Rev. D* **62**, 033007 (2000) [arXiv:hep-ph/9907423].
- [20] C. Lunardini and A. Y. Smirnov, “Supernova neutrinos: Earth matter effects and neutrino mass spectrum,” *Nucl. Phys. B* **616**, 307 (2001) [arXiv:hep-ph/0106149].
- [21] K. Takahashi and K. Sato, “Earth effects on supernova neutrinos and their implications for neutrino parameters,” *Phys. Rev. D* **66**, 033006 (2002) [arXiv:hep-ph/0110105].
- [22] A. S. Dighe, M. T. Keil and G. G. Raffelt, “Identifying earth matter effects on supernova neutrinos at a single detector,” *JCAP* **0306**, 006 (2003) [arXiv:hep-ph/0304150].
- [23] A. S. Dighe, M. Kachelrieß, G. G. Raffelt and R. Tomas, “Signatures of supernova neutrino oscillations in the earth mantle and core,” *JCAP* **0401**, 004 (2004) [arXiv:hep-ph/0311172].
- [24] C. Lunardini and A. Y. Smirnov, “Probing the neutrino mass hierarchy and the 13-mixing with supernovae,” *JCAP* **0306**, 009 (2003) [arXiv:hep-ph/0302033].
- [25] A. Mirizzi, G. G. Raffelt and P. D. Serpico, “Earth matter effects in supernova neutrinos: Optimal detector locations,” *JCAP* **0605**, 012 (2006) [arXiv:astro-ph/0604300].
- [26] J. T. Pantaleone, “Neutrino oscillations at high densities,” *Phys. Lett. B* **287**, 128 (1992).
- [27] S. Samuel, “Neutrino oscillations in dense neutrino gases,” *Phys. Rev. D* **48**, 1462 (1993).
- [28] Y. Z. Qian and G. M. Fuller, “Matter enhanced anti-neutrino flavor transformation and supernova nucleosynthesis,” *Phys. Rev. D* **52**, 656 (1995) [arXiv:astro-ph/9502080].
- [29] S. Pastor and G. Raffelt, “Flavor oscillations in the supernova hot bubble region: Nonlinear effects of neutrino background,” *Phys. Rev. Lett.* **89**, 191101 (2002) [arXiv:astro-ph/0207281].
- [30] R. F. Sawyer, “Speed-up of neutrino transformations in a supernova environment,” *Phys. Rev. D* **72**, 045003 (2005) [arXiv:hep-ph/0503013].
- [31] G. M. Fuller and Y. Z. Qian, “Simultaneous flavor transformation of neutrinos and antineutrinos with dominant potentials from neutrino neutrino forward scattering,” *Phys. Rev. D* **73**, 023004 (2006) [arXiv:astro-ph/0505240].
- [32] H. Duan, G. M. Fuller and Y. Z. Qian, “Collective neutrino flavor transformation in supernovae,” *Phys. Rev. D* **74**, 123004 (2006) [arXiv:astro-ph/0511275].
- [33] H. Duan, G.M. Fuller, J. Carlson and Y.Z. Qian, “Simulation of coherent non-linear neutrino flavor transformation in the supernova environment. I: Correlated neutrino trajectories,” *Phys. Rev. D* **74**, 105014 (2006) [arXiv:astro-ph/0606616].
- [34] S. Hannestad, G. G. Raffelt, G. Sigl and Y. Y. Y. Wong, “Self-induced conversion in dense neutrino gases: Pendulum in flavor space,” *Phys. Rev. D* **74**, 105010 (2006); Erratum *ibid.* **76**, 029901 (2007) [arXiv:astro-ph/0608695].

- [35] H. Duan, G. M. Fuller, J. Carlson and Y. Z. Qian, “Analysis of collective neutrino flavor transformation in supernovae,” *Phys. Rev. D* **75**, 125005 (2007) [arXiv:astro-ph/0703776].
- [36] G. G. Raffelt and G. Sigl, “Self-induced decoherence in dense neutrino gases,” *Phys. Rev. D* **75**, 083002 (2007) [arXiv:hep-ph/0701182].
- [37] A. Esteban-Pretel, S. Pastor, R. Tomàs, G. G. Raffelt and G. Sigl, “Decoherence in supernova neutrino transformations suppressed by deleptonization,” *Phys. Rev. D* **76**, 125018 (2007) [arXiv:0706.2498 [astro-ph]].
- [38] G. G. Raffelt and A. Yu. Smirnov, “Self-induced spectral splits in supernova neutrino fluxes,” *Phys. Rev. D* **76**, 081301 (2007) [arXiv:0705.1830 [hep-ph]].
- [39] G. G. Raffelt and A. Yu. Smirnov, “Adiabaticity and spectral splits in collective neutrino transformations,” *Phys. Rev. D* **76**, 125008 (2007) [arXiv:0709.4641 [hep-ph]].
- [40] H. Duan, G. M. Fuller and Y. Z. Qian, “A simple picture for neutrino flavor transformation in supernovae,” *Phys. Rev. D* **76**, 085013 (2007) [arXiv:0706.4293 [astro-ph]].
- [41] H. Duan, G. M. Fuller, J. Carlson and Y. Z. Qian, “Neutrino mass hierarchy and stepwise spectral swapping of supernova neutrino flavors,” *Phys. Rev. Lett.* **99**, 241802 (2007) [arXiv:0707.0290 [astro-ph]].
- [42] G. L. Fogli, E. Lisi, A. Marrone and A. Mirizzi, “Collective neutrino flavor transitions in supernovae and the role of trajectory averaging,” *JCAP* **0712**, 010 (2007) [arXiv:0707.1998 [hep-ph]].
- [43] H. Duan, G. M. Fuller, J. Carlson and Y. Z. Qian, “Flavor evolution of the neutronization neutrino burst from an O-Ne-Mg core-collapse supernova,” *Phys. Rev. Lett.* **100**, 021101 (2008) [arXiv:0710.1271 [astro-ph]].
- [44] B. Dasgupta, A. Dighe, A. Mirizzi and G. G. Raffelt, “Spectral split in prompt supernova neutrino burst: Analytic three-flavor treatment,” *Phys. Rev. D* **77**, 113007 (2008) [arXiv:0801.1660 [hep-ph]].
- [45] C. Lunardini, B. Muller and H. T. Janka, “Neutrino oscillation signatures of oxygen-neon-magnesium supernovae,” *Phys. Rev. D* **78** (2008) 023016 [arXiv:0712.3000 [astro-ph]].
- [46] A. Esteban-Pretel, S. Pastor, R. Tomàs, G. G. Raffelt and G. Sigl, “Mu-tau neutrino refraction and collective three-flavor transformations in supernovae,” *Phys. Rev. D* **77**, 065024 (2008) [arXiv:0712.1137 [astro-ph]].
- [47] B. Dasgupta and A. Dighe “Collective three-flavor oscillations of supernova neutrinos,” *Phys. Rev. D* **77**, 113002 (2008) [arXiv:0712.3798 [hep-ph]].
- [48] H. Duan, G. M. Fuller and Y. Z. Qian, “Stepwise spectral swapping with three neutrino flavors,” *Phys. Rev. D* **77**, 085016 (2008) [arXiv:0801.1363 [hep-ph]].
- [49] B. Dasgupta, A. Dighe and A. Mirizzi, “Identifying neutrino mass hierarchy at extremely small  $\theta_{13}$  through Earth matter effects in a supernova signal,” *Phys. Rev. Lett.* **101**, 171801 (2008) [arXiv:0802.1481 [hep-ph]].
- [50] R. F. Sawyer, “The multi-angle instability in dense neutrino systems,” *Phys. Rev. D* **79**, 105003 (2009) [arXiv:0803.4319 [astro-ph]].
- [51] H. Duan, G. M. Fuller and J. Carlson, “Simulating nonlinear neutrino flavor evolution,” *Comput. Sci. Dis.* **1**, 015007 (2008) [arXiv:0803.3650 [astro-ph]].
- [52] S. Chakraborty, S. Choubey, B. Dasgupta and K. Kar, “Effect of Collective Flavor Oscillations on the Diffuse Supernova Neutrino Background,” *JCAP* **0809**, 013 (2008) [arXiv:0805.3131 [hep-ph]].
- [53] B. Dasgupta, A. Dighe, A. Mirizzi and G. G. Raffelt, “Collective neutrino oscillations in non-spherical geometry,” *Phys. Rev. D* **78**, 033014 (2008) [arXiv:0805.3300 [hep-ph]].
- [54] A. Esteban-Pretel, A. Mirizzi, S. Pastor, R. Tomas, G. G. Raffelt, P. D. Serpico and G. Sigl, “Role of dense matter in collective supernova neutrino transformations,” *Phys. Rev. D* **78**, 085012 (2008) [arXiv:0807.0659 [astro-ph]].
- [55] J. Gava and C. Volpe, “Collective neutrinos oscillation in matter and CP-violation,” *Phys. Rev. D* **78**, 083007 (2008) [arXiv:0807.3418 [astro-ph]].
- [56] G. L. Fogli, E. Lisi, A. Marrone, A. Mirizzi and I. Tamborra, “Low-energy spectral features of supernova (anti)neutrinos in inverted hierarchy,” *Phys. Rev. D* **78**, 097301 (2008) [arXiv:0808.0807 [hep-ph]].
- [57] H. Duan, G. M. Fuller and Y. Z. Qian, “Symmetries in collective neutrino oscillations,” *J. Phys. G* **36**, 105003 (2009) [arXiv:0808.2046 [astro-ph]].
- [58] G. G. Raffelt, “Self-induced parametric resonance in collective neutrino oscillations,” *Phys. Rev. D* **78**, 125015 (2008) [arXiv:0810.1407 [hep-ph]].
- [59] M. Blennow, A. Mirizzi and P. D. Serpico, “Non-standard neutrino-neutrino refractive effects in dense neutrino gases,” *Phys. Rev. D* **78**, 113004 (2008) [arXiv:0810.2297 [hep-ph]].
- [60] G. Fogli, E. Lisi, A. Marrone and I. Tamborra, “Supernova neutrino three-flavor evolution with dominant collective effects,” *JCAP* **0904**, 030 (2009) [arXiv:0812.3031 [hep-ph]].
- [61] J. Gava, J. Kneller, C. Volpe and G. C. McLaughlin, “A dynamical collective calculation of supernova neutrino signals,” *Phys. Rev. Lett.* **103**, 071101 (2009) [arXiv:0902.0317 [hep-ph]].
- [62] B. Dasgupta, A. Dighe, G. G. Raffelt and A. Y. Smirnov, “Multiple Spectral Splits of Supernova Neutrinos,” *Phys. Rev. Lett.* **103**, 051105 (2009) [arXiv:0904.3542 [hep-ph]].
- [63] G. Fogli, E. Lisi, A. Marrone and I. Tamborra, “Supernova neutrinos and antineutrinos: ternary luminosity diagram and spectral split patterns,” *JCAP* **0910** (2009) 002 [arXiv:0907.5115 [hep-ph]].
- [64] S. Galais, J. Kneller, C. Volpe and J. Gava, “Shockwaves in Supernovae: New Implications on the Diffuse Supernova Neutrino Background,” *Phys. Rev. D* **81**, 053002 (2010) [arXiv:0906.5294 [hep-ph]].
- [65] A. Mirizzi, S. Pozzorini, G. G. Raffelt and P. D. Serpico, “Flavour-dependent radiative correction to neutrino-neutrino refraction,” *JHEP* **0910**, 020 (2009) [arXiv:0907.3674 [hep-ph]].
- [66] A. Esteban-Pretel, R. Tomas and J. W. F. Valle, “Interplay between collective effects and non-standard neutrino interactions of supernova neutrinos,” *Phys. Rev. D* **81**, 063003 (2010) [arXiv:0909.2196 [hep-ph]].
- [67] S. Chakraborty, S. Choubey, S. Goswami and K. Kar, “Collective Flavor Oscillations Of Supernova Neutrinos and r-Process Nucleosynthesis,” [arXiv:0911.1218 [hep-ph]].
- [68] H. Duan, G. M. Fuller and Y. Z. Qian, “Collective Neutrino Oscillations,” [arXiv:1001.2799 [hep-ph]].
- [69] B. Dasgupta, G. G. Raffelt and I. Tamborra, “Triggering collective oscillations by three-flavor effects,” *Phys.*



- Rev. D **81**, 073004 (2010) [arXiv:1001.5396 [hep-ph]].
- [70] A. Friedland, “Self-refraction of supernova neutrinos: mixed spectra and three-flavor instabilities,” Phys. Rev. Lett. **104**, 191102 (2010) [arXiv:1001.0996 [hep-ph]].
- [71] B. Dasgupta, A. Mirizzi, I. Tamborra and R. Tomas, “Neutrino mass hierarchy and three-flavor spectral splits of supernova neutrinos,” Phys. Rev. D **81**, 093008 (2010) [arXiv:1002.2943 [hep-ph]].
- [72] H. Duan and A. Friedland, “Self-induced suppression of collective neutrino oscillations in a supernova,” [arXiv:1006.2359 [hep-ph]].
- [73] J. F. Cherry, G. M. Fuller, J. Carlson, H. Duan and Y. Z. Qian, “Multi-Angle Simulation of Flavor Evolution in the Neutrino Neutronization Burst From an O-Ne-Mg Core-Collapse Supernova,” [arXiv:1006.2175 [astro-ph.HE]].
- [74] T. Totani, K. Sato, H. E. Dalhed and J. R. Wilson, “Future detection of supernova neutrino burst and explosion mechanism,” Astrophys. J. **496**, 216 (1998) [arXiv:astro-ph/9710203].
- [75] R. Buras, H. T. Janka, M. T. Keil, G. G. Raffelt and M. Rampp, “Electron-neutrino pair annihilation: A new source for muon and tau neutrinos in supernovae,” Astrophys. J. **587**, 320 (2003) [arXiv:astro-ph/0205006].
- [76] M. T. Keil, G. G. Raffelt and H. T. Janka, “Monte Carlo study of supernova neutrino spectra formation,” Astrophys. J. **590**, 971 (2003) [arXiv:astro-ph/0208035].
- [77] G. G. Raffelt, M. T. Keil, R. Buras, H. T. Janka and M. Rampp, “Supernova neutrinos: Flavor-dependent fluxes and spectra,” [arXiv:astro-ph/0303226].
- [78] T. Fischer, S. C. Whitehouse, A. Mezzacappa, F. K. Thielemann and M. Liebendorfer, “Protoneutron star evolution and the neutrino driven wind in general relativistic neutrino radiation hydrodynamics simulations,” [arXiv:0908.1871 [astro-ph.HE]].
- [79] L. Hudepohl, B. Muller, H. T. Janka, A. Marek and G. G. Raffelt, “Neutrino Signal of Electron-Capture Supernovae from Core Collapse to Cooling,” Phys. Rev. Lett. **104**, 251101 (2010) [arXiv:0912.0260 [astro-ph.SR]].
- [80] C. K. Jung, “Feasibility of a next generation underground water Cherenkov detector: UNO,” AIP Conf. Proc. **533**, 29 (2000) [arXiv:hep-ex/0005046].
- [81] K. Nakamura, “Hyper-Kamiokande: A next generation water Cherenkov detector,” Int. J. Mod. Phys. A **18**, 4053 (2003).
- [82] A. de Bellefon *et al.*, “MEMPHYS: A large scale water Cherenkov detector at Frejus,” [arXiv:hep-ex/0607026].
- [83] M. D. Kistler, H. Yuksel, S. Ando, J. F. Beacom and Y. Suzuki, “Core-Collapse Astrophysics with a Five-Megaton Neutrino Detector,” [arXiv:0810.1959 [astro-ph]].
- [84] T. Marrodan Undagoitia *et al.*, “LENA: A multipurpose detector for low energy neutrino astronomy and proton D. J. Phys. Conf. Ser. **120**, 052018 (2008).
- [85] D. B. Cline, F. Raffaelli and F. Sergiampietri, “LAN-NDD: A line of liquid argon TPC detectors scalable in mass from 200-tons to 100-kts,” JINST **1**, T09001 (2006) [arXiv:astro-ph/0604548].
- [86] A. Badertscher *et al.*, “A Possible Future Long Baseline Neutrino and Nucleon Decay Experiment with a 100 kt Liquid Argon TPC at Okinoshima using the J-PARC Neutrino Facility,” [arXiv:0804.2111 [hep-ph]].
- [87] A. Ereditato and A. Rubbia, “The liquid argon TPC: A powerful detector for future neutrino experiments and proton decay searches,” Nucl. Phys. Proc. Suppl. **154**, 163 (2006) [arXiv:hep-ph/0509022].
- [88] B. Baibussinov *et al.*, “A new, very massive modular Liquid Argon Imaging Chamber to detect low energy off-axis neutrinos from the CNGS beam. (Project MODULAR),” Astropart. Phys. **29**, 174 (2008) [arXiv:0704.1422 [hep-ph]].
- [89] D. Autiero *et al.*, “Large underground, liquid based detectors for astro-particle physics in Europe: scientific case and prospects,” JCAP **0711**, 011 (2007) [arXiv:0705.0116 [hep-ph]].
- [90] M. C. Sanchez [LBNE DUSEL Collaboration], “A Very Long-Baseline Neutrino Experiment from FNAL to DUSEL,” AIP Conf. Proc. **1222**, 479 (2010).
- [91] M. T. Keil, “Supernova neutrino spectra and applications to flavor oscillations,” Ph.D Thesis, [arXiv:astro-ph/0308228].
- [92] G. Sigl and G. Raffelt, “General kinetic description of relativistic mixed neutrinos,” Nucl. Phys. B **406**, 423 (1993).
- [93] F. J. Botella, C. S. Lim and W. J. Marciano, “Radiative corrections to neutrino indices of refraction,” Phys. Rev. D **35**, 896 (1987).
- [94] M. C. Gonzalez-Garcia, M. Maltoni and J. Salvado, “Updated global fit to three neutrino mixing: status of the hints of  $\theta_{13} > 0$ ,” JHEP **1004**, 056 (2010) [arXiv:1001.4524 [hep-ph]].
- [95] G. L. Fogli, E. Lisi, D. Montanino and A. Palazzo, “Supernova neutrino oscillations: A simple analytical approach,” Phys. Rev. D **65**, 073008 (2002) [Erratum-ibid. D **66**, 039901 (2002)] [arXiv:hep-ph/0111199].
- [96] A. Strumia and F. Vissani, “Precise quasielastic neutrino nucleon cross section,” Phys. Lett. B **564**, 42 (2003) [arXiv:astro-ph/0302055].
- [97] R. Tomas, D. Semikoz, G. G. Raffelt, M. Kachelrieß and A. S. Dighe, “Supernova pointing with low- and high-energy neutrino detectors,” Phys. Rev. D **68**, 093013 (2003) [arXiv:hep-ph/0307050].
- [98] M. Wurm, F. von Feilitzsch, M. Goeger-Neff, K. A. Hochmuth, T. M. Undagoitia, L. Oberauer and W. Potzel, “Detection potential for the diffuse supernova neutrino background in the large liquid-scintillator detector LENA,” Phys. Rev. D **75**, 023007 (2007) [arXiv:astro-ph/0701305].
- [99] L. Oberauer, private communication.
- [100] A. G. Cocco, A. Ereditato, G. Fiorillo, G. Mangano and V. Pettorino, “Supernova relic neutrinos in liquid argon detectors,” JCAP **0412**, 002 (2004) [arXiv:hep-ph/0408031].
- [101] I. Gil-Botella and A. Rubbia, “Oscillation effects on supernova neutrino rates and spectra and detection of the shock breakout in a liquid argon TPC,” JCAP **0310**, 009 (2003) [arXiv:hep-ph/0307244].
- [102] I. Gil-Botella and A. Rubbia, “Decoupling supernova and neutrino oscillation physics with LAr TPC detectors,” JCAP **0408**, 001 (2004) [arXiv:hep-ph/0404151].
- [103] A. S. Dighe, M. T. Keil and G. G. Raffelt, “Detecting the neutrino mass hierarchy with a supernova at IceCube,” JCAP **0306**, 005 (2003) [arXiv:hep-ph/0303210].
- [104] M. Kachelrieß, R. Tomas, R. Buras, H. T. Janka, A. Marek and M. Rampp, “Exploiting the neutronization burst of a galactic supernova,” Phys. Rev. D **71**,

- 063003 (2005) [arXiv:astro-ph/0412082].
- [105] Y. Y. Y. Wong, “Analytical treatment of neutrino asymmetry equilibration from flavour oscillations in the early universe,” *Phys. Rev. D* **66**, 025015 (2002) [arXiv:hep-ph/0203180].
- [106] G. Pagliaroli, F. Vissani, E. Coccia and W. Fulgione, “Neutrinos from Supernovae as a Trigger for Gravitational Wave Search,” *Phys. Rev. Lett.* **103**, 031102 (2009) [arXiv:0903.1191 [hep-ph]].
- [107] F. Halzen and G. G. Raffelt, “Reconstructing the supernova bounce time with neutrinos in IceCube,” *Phys. Rev. D* **80**, 087301 (2009) [arXiv:0908.2317 [astro-ph.HE]].
- [108] B. Dasgupta, T. Fischer, S. Horiuchi, M. Liebendorfer, A. Mirizzi, I. Sagert and J. Schaffner-Bielich, “Detecting the QCD phase transition in the next Galactic supernova neutrino burst,” *Phys. Rev. D* **81**, 103005 (2010) [arXiv:0912.2568 [astro-ph.HE]].
- [109] T. Lund, A. Marek, C. Lunardini, H. T. Janka and G. Raffelt, “Fast time variations of supernova neutrino fluxes and their detectability,” [arXiv:1006.1889 [astro-ph.HE]].